FOREWORD

ABSTRACT

1. Vaporization Studies

    a. Iridium, Rhodium, and Ruthenium

        1) Iridium

The vaporization of iridium has been studied by Knudsen effusion and Langmuir evaporation techniques. The vapor pressure of iridium over the temperature range of from 2100° to 2600°K is represented by the equation:

$$\log_{10} P_{mm} = 10.46 - \frac{33,980}{T} \; .$$

Third law analyses of the data yield an average heat of vaporization: $\Delta H^\circ_{298} = 158.4 \pm 0.5 \, kcal/mole$. The estimated boiling point of iridium is 4800°K.

        2) Rhodium

The previously reported raw data for rhodium have been analyzed. The vapor pressure of rhodium for the temperature range of 2050° to 2200°K is represented by the equation:

$$\log_{10} P_{mm} = 10.28 - \frac{28,300}{T} \; .$$

Third law analyses of the data yield an average heat of vaporization: $\Delta H^\circ_{298} = 132.8 \pm 0.3 \, kcal/mole$.

        3) Ruthenium

The vaporization of ruthenium has been studied by a Knudsen effusion technique. Tentative data for the vapor pressure from the temperature range of 2000° to 2500°K have been obtained. These data are represented by the equation:

$$\log_{10} P_{mm} = 10.76 - \frac{33,550}{T} \; .$$

Third law analyses of the data yield an average heat of vaporization: $\Delta H^\circ_{298} = 155.7 \pm 1.7 \, kcal/mole$. The boiling point estimated from these data is 4400°K.

b. Iridium-Carbon

The vapor pressure of iridium, vaporized from a graphite effusion cell, was found to be as much as several orders of magnitude lower than that of pure iridium.
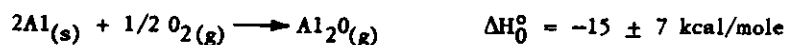
c. Alumina (Al_2O_3)

The study of the vaporization of Al_2O_3 was essentially completed. In both iridium and tungsten cells, the principal mode of vaporization was:

$$Al_2O_3 \longrightarrow 2Al_{(g)} + 3O_{(g)},$$
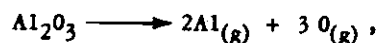
where the Al_2O_3 is in either the solid or the liquid state. In iridium effusion cells, small amounts of AlO and Al_2O were observed. These species, as well as WO_2, were also observed in small amounts during tests in tungsten effusion cells.

Calculations with the data from this work and available spectroscopic data yielded the following information for the gaseous oxides of aluminium:

$$Al_2O_{(g)} \longrightarrow 2Al_{(g)} + O_{(g)} \qquad \Delta H_0^\circ = 230 \pm 7 \text{ kcal/mole}$$

$$AlO_{(g)} \longrightarrow Al_{(g)} + O_{(g)} \qquad \Delta H_0^\circ = 105 \pm 5 \text{ kcal/mole}$$

$$2Al_{(s)} + 1/2\, O_{2(g)} \longrightarrow Al_2O_{(g)} \qquad \Delta H_0^\circ = -15 \pm 7 \text{ kcal/mole}$$

$$Al_{(s)} + 1/2\, O_{2(g)} \longrightarrow AlO_{(g)} \qquad \Delta H_0^\circ = 32 \pm 5 \text{ kcal/mole}$$

$$Al_2O_{(g)} \longrightarrow Al_{(g)} + AlO_{(g)} \qquad \Delta H_0^\circ = 125 \pm 12 \text{ kcal/mole} \quad .$$
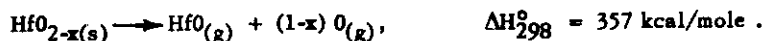
d. Thoria

Experimental difficulties were encountered in the study of the vaporization of thoria, specifically with effustion techniques and mass spectrometry. Although it appeared that $ThO_{(g)}$ might have been present in appreciable quantities, in addition to the major constituent $ThO_{2(g)}$ in the equilibrium gas, this point was not settled.

e.   Hafnia

Mass spectrometric studies of the vaporization of hafnia showed that the major vaporizing oxide species was $HfO_{(g)}$. It appeared, on the basis of the experimental data that the vaporization of hafnia was not stoichiometric, and that a small amount of oxygen was lost.

Simple effusion studies yielded the following approximate results:
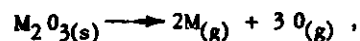
$$HfO_{2(s)} \longrightarrow HfO_{(g)} + O_{(g)} , \qquad \Delta H^o_{298} = 347 \text{ kcal/mole}$$

$$HfO_{2-x(s)} \longrightarrow HfO_{(g)} + (1-x) O_{(g)} , \qquad \Delta H^o_{298} = 357 \text{ kcal/mole} .$$

f.   The Vaporization of the Rare Earth Sesquioxides

The rare earth sesquioxides may be divided into two groups on the basis of a plot of I_{M+}/I_{MO+} versus atomic number of the metal; within each, the major vaporization mode changes from:

$$M_2O_{3(s)} \longrightarrow 2MO_{(g)} + O_{(g)} ,$$

to

$$M_2O_{3(s)} \longrightarrow 2M_{(g)} + 3 O_{(g)} ,$$
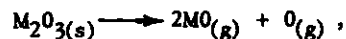
with increasing atomic number of the rare earth metal.

g.   Continuously Monitored Effusion Experiments

   1)   Mo - Si System

   Continuously monitored effusion experiments, performed by effusing silicon from a molybdenum crucible containing silicon powder, have yielded the following heats of dissociation in kcal/gram atom of silicon at 298°K:

   Two phase region, Liquid $MoSi_2$ 117.8;

   Two phase region, $MoSi_2$, Mo_5Si_3 ....121.5;

   Two phase region, Mo_5Si_3 , Mo_3Si ....128.3; and

Two-phase region, Mo_3Si, Mo 132.9

2) W-Si System

Continuously monitored effusion experiments, performed in tungsten crucibles, have yielded the following approximate dissociation pressures at ~ 1765°K:

Two phase region, liquid WSi_2 ....3.5×10^{-6}atm,

Two phase region, $WSi_2 - W_3Si_2$ ....2.6×10^{-6}atm,

Two phase region, $W_3Si_2 - W$ ....1.7×10^{-6}atm.

3) Ta - B System

Although several experiments have been run, no useful data have been obtained.
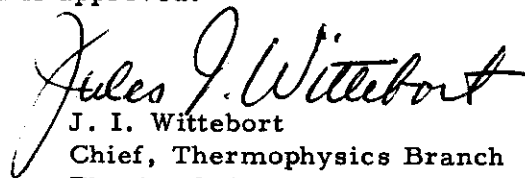
2. Surface Tension

The surface tensions of silica and silica plus 1 percent oxide additives, and zirconium plus uranium have been measured by a sessile drop technique.

3. Viscosity

The viscosities of the following materials have been measured: alumina (~ 1 to 10 poises), Zr plus 10 percent U (~1.5 poises), silica, silica plus 1 percent V_2O_5 , silica plus 1 percent CoO , and silica plus 1 percent Al_2O_3 .

This report has been reviewed and is approved.

J. I. Wittebort
Chief, Thermophysics Branch
Physics Laboratory
Directorate of Materials and Processes

TABLE OF CONTENTS

LIST OF FIGURES

LIST OF FIGURES (Concl'd)

LIST OF TABLES

I. VAPORIZATION STUDIES

The experimental techniques, used for the study of vaporization of several refractory materials in this contract, have been described in detail (ref. 1). The method of effusion cell heating, in simple effusion and mass spectrometric studies, is described in appendix A. Further detailed descriptions will be given only where they differ substantially from those already reported.

A. THE VAPORIZATION OF IRIDIUM, RHODIUM, AND RUTHENIUM

1. Iridium and Rhodium

Experimental details and data for Knudsen effusion studies of vaporization of iridium have already been reported (ref. 1). The data included experimental points obtained when thoria effusion cells with 1/16 and 1/8 in. orifices were used. The data were reported to be in doubt, and the results obtained with 1/16 in. orifices were found to differ from those obtained with 1/8 in. orifices.

Subsequent examination of the cells, used for these studies, revealed that the data obtained with the 1/8 in. orifice were not correct. This was due to geometric factors, discussed in appendix B. To check the effusion data obtained with the 1/16 in. orifice, a Langmuir vaporization experiment was performed.

A complete discussion of the vaporization studies of iridium and rhodium has been prepared for publication and is given in appendix B. The experimental data for rhodium found in appendix B were given in the previous report in this series (ref. 1), but third law calculations were not included at the time.

2. Ruthenium

The experimental techniques used for the effusion studies of the vaporization of ruthenium were the same as those described in appendix B for iridium and rhodium. In most of the experiments, the quantity of ruthenium that had been deposited upon the targets was determined by the use of Ru^{103} as a radioactive tracer. The radioactivity of the target, upon which the effusion beam condensed, was compared with that of a previously calibrated sample. This sample contained the same ratio of tracer to natural isotopes and a known total weight of the reference material.

The labeled ruthenium was prepared by adding the required amount of $Ru^{103}Cl_3$ (obtained from Oak Ridge National Laboratory in HCl solution) to an aqueous solution of nonradioactive $RuCl_3$ of known concentration. The solution was then evaporated to dryness and heated to approximately 700°C in a stream of hydrogen, thus reducing the $RuCl_3$ to Ru metal.

In these effusion experiments, the thoria-lined effusion cells were almost identical to that shown in figure 4. The cells were modified in the sense that orifices of 1/8, 1/16 and 1/32 in. (nominal diameter) were used. The iridium liner was, of course, removed.

Two groups of experiments were carried out:

a. Cells with orifice diameters of 1/8 in. and a charge of natural ruthenium metal powder were used. The amount of material deposited on the targets was determined by weighing. The data obtained from these runs were very scattered. In general, the higher temperature points fell above a linear $\log P$ versus $1/T$ plot of the lower temperature data. When these experiments were done, in cases where the amount of material could be checked with a radioactive tracer, it was found that the weight change did not correspond to the amount of ruthenium deposited on the target. A much greater amount of material was found to have been deposited.

In an earlier report, it had been indicated that thoria appeared to vaporize at an increased rate after being heated for a short period of time in tungsten. The difficulties encountered in these studies appear to be directly related to the latter effect. The data obtained in these experiments were rejected.

b. Cells with nominal orifice diameters of 1/8, 1/16 and 1/32 in., were used with a charge of labeled ruthenium metal, as described above. The pressures obtained with the 1/8 in. orifice were appreciably lower than those obtained with 1/16 and 1/32 in. orifices. The data obtained with the 1/8 in. orifice have been rejected, but the line that represented the data is included for comparison in figure 1, along with the other ruthenium effusion data.

The effusion data obtained when 1/16 and 1/32 in. orifices were used are rather scattered, but as seen in figure 1 they appear to scatter approximately about one line. The solid line that was drawn through all the 1/16 and 1/32 in. data points was determined by a third law analysis, in the manner described for iridium in appendix B. Points for the runs in which 1/16 and 1/32 in. orifices were used were given equal weight. The data are represented by the equation:

$$\log_{10} P_{mm} = 10.76 - \frac{33,550}{T} \ . \tag{1}$$
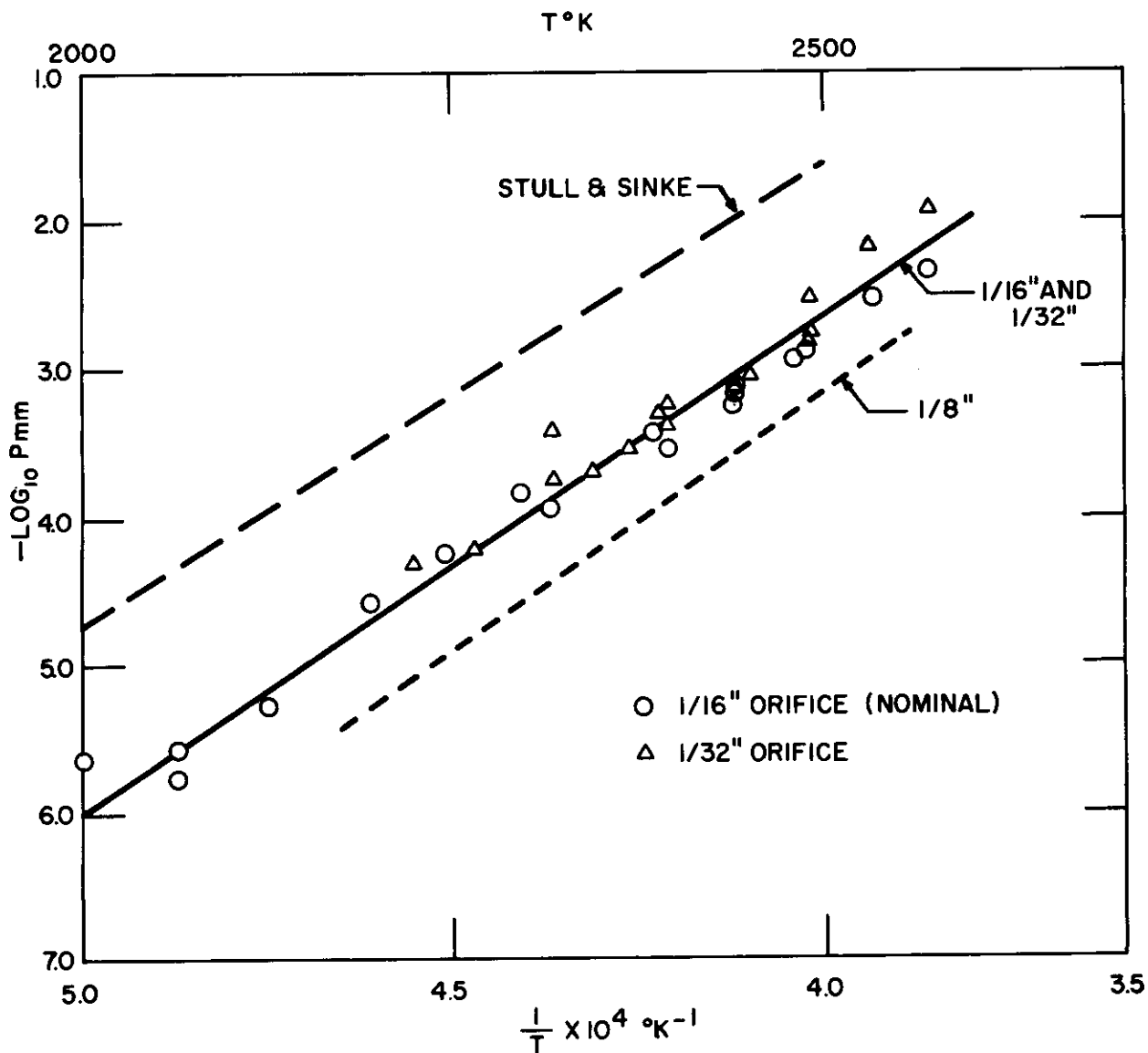
Figure 1 Log P versus 1/T for the vaporization of ruthenium

It is assumed that the linear equation holds for the temperature range of 2000° to $2500^\circ K$.

In Table 1, the vapor pressures obtained experimentally, using 1/16 and 1/32 in. effusion cells, are given, along with free energy functions from Stull and Sinke (ref. 2) and heats of vaporization calculated on the basis of third law data. The ΔH°_{298}, calculated from the data obtained with the 1/16 in. orifice, is 156.3 ± 1.3 (average deviation) kcal/mole, and that for the data obtained with the 1/32 in. orifice, is 155.0 ± 1.7 kcal/mole. The average ΔH°_{298} for all points is 155.7 ± 1.7 kcal/mole.

The boiling point of ruthenium was calculated by estimating the average heat of vaporization for liquid ruthenium from the melting point to $4500^\circ K$. This quantity was used with the estimated vapor pressure at the melting point and the integrated Clausius-Clapeyron equation to obtain a boiling point of approximately $4400^\circ K$.

The data reported above should be considered tentative, since there was a possibility of interference by thoria species, resulting from interaction between thoria and tungsten. The effusion data should be checked by a Langmuir experiment, similar to that done in the study of the vaporization of iridium.

B. VAPORIZATION OF IRIDIUM IN THE PRESENCE OF CARBON

Radioactive iridium was studied in a graphite liner placed inside a tungsten effusion cell similar to that shown in figure 22. Samples were collected by techniques that have been described for the studies of the vaporization of iridium and rhodium in appendix B. The species effusing from the cell has been identified mass spectrometrically as monatomic iridium.

The simple effusion data are given in Table 2 and are compared with the equilibrium data for pure iridium (see figure 2). At the start of each run, the measured vapor pressure of the iridium in the graphite crucible was near that of pure iridium (as shown by points A and B in figure 2; these were the first experimental points obtained in each of two runs). After a short period of heating, the iridium pressure inside the crucible dropped to that shown by the triangles. At some point in the run, the iridium sample melted. The scatter in the data may be due to inhomogeneity or changing composition of the sample.

The vapor pressure of the iridium was reduced from one to two orders of magnitude by the presence of carbon. This indicates that there is either reaction between carbon and iridium, or extensive solution formation. No surface coating was observed on the iridium.

T°K

2000　　　　　　　　　　　2500

VAPOR PRESSURE OF PURE Ir

△　　VAPOR PRESSURE OF Ir IN GRAPHITE

$-\log_{10} P_{mm}$

O (B)

O (A)
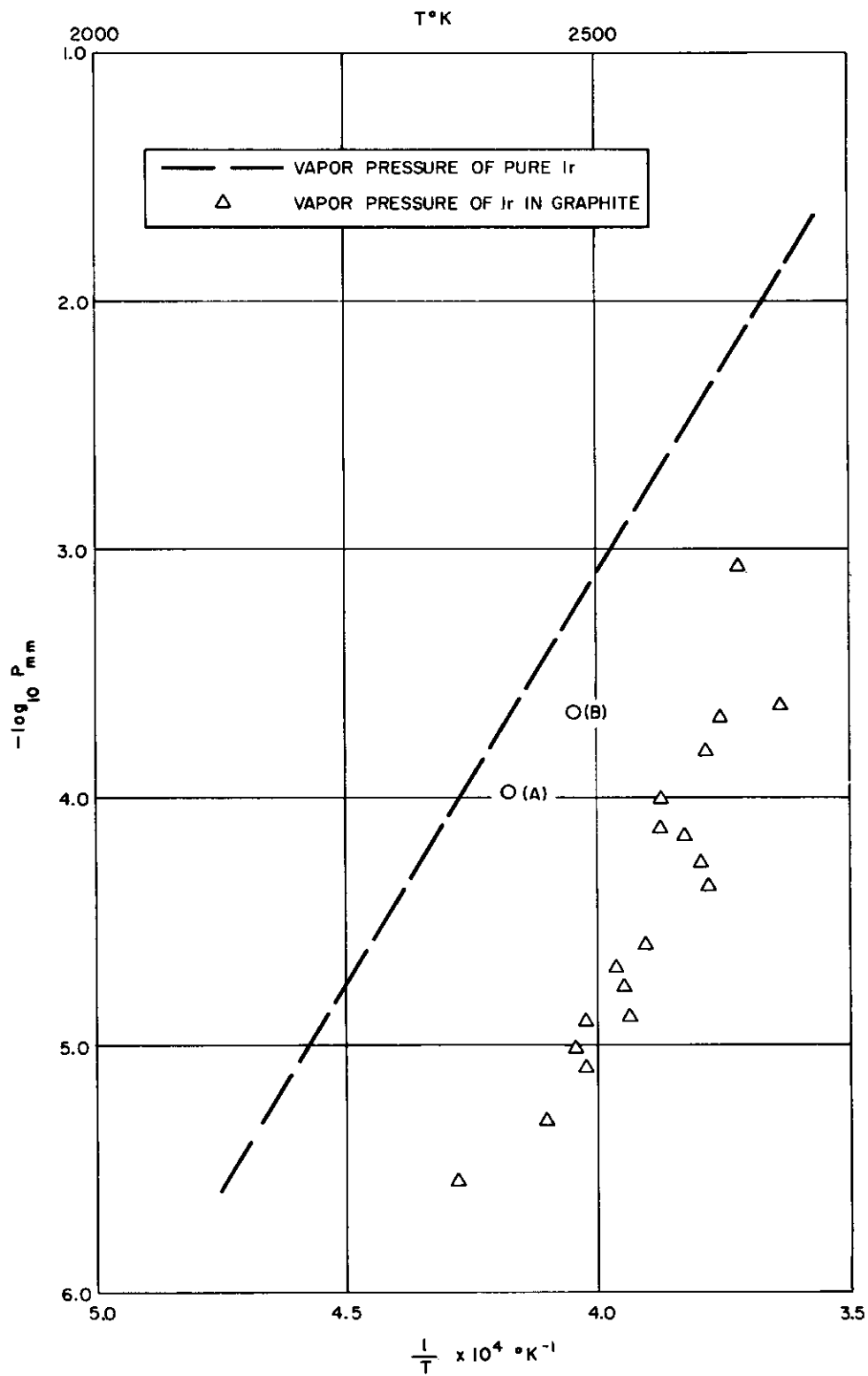
$\frac{1}{T} \times 10^4 \ °K^{-1}$

Figure 2　Vaporization of iridium in the presence of carbon

TABLE 1. THE VAPORIZATION OF RUTHENIUM

T °K	$1/T \times 10^4$ °K^{-1}	$-\log P_{mm}$	fef$_{(s)}$* eu	fef$_{(g)}$* eu	$-\Delta$fef eu	ΔH_{298} kcal/mole
			(1/16 in. Orifice)			
1998	5.01	5.63	13.53	50.69	37.16	152.0
2053	4.87	5.78	13.69	50.83	37.14	157.6
2053	4.87	5.59	13.69	50.83	37.14	155.8
2106	4.75	5.29	13.84	50.97	37.13	156.9
2170	4.61	4.59	14.02	51.13	37.11	154.7
2219	4.51	4.26	14.16	51.25	37.09	154.8
2268	4.41	3.84	14.29	51.36	37.07	153.8
2289	4.37	3.96	14.35	51.41	37.06	156.5
2365	4.23	3.44	14.56	51.59	37.03	156.0
2375	4.21	3.57	14.58	51.61	37.03	158.0
2429	4.12	3.26	14.73	51.74	37.01	158.1
2429	4.12	3.18	14.73	51.74	37.01	157.3
2429	4.12	3.16	14.73	51.74	37.01	157.0
2472	4.05	2.95	14.84	51.83	36.99	157.4
2483	4.03	2.90	14.87	51.86	36.99	157.5
2542	3.93	2.54	15.02	51.99	36.97	157.0
2590	3.86	2.35	15.13	52.09	36.96	157.7
			(1/32 in. Orifice)			
2203	4.55	4.29	14.11	51.21	37.10	154.0
2235	4.47	4.24	14.20	51.28	37.08	155.7
2289	4.37	3.42	14.35	51.41	37.06	150.8
2289	4.37	3.76	14.35	51.41	37.06	154.4
2322	4.31	3.71	14.44	51.49	37.05	156.0
2343	4.27	3.55	14.49	51.54	37.05	154.4
2375	4.21	3.24	14.59	51.61	37.02	154.4
2375	4.21	3.31	14.59	51.61	37.02	155.2
2375	4.21	3.41	14.59	51.61	37.02	156.3
2429	4.12	3.09	14.73	51.74	37.01	156.2
2429	4.12	3.15	14.73	51.74	37.01	159.6
2483	4.03	2.52	14.87	51.86	36.99	153.2
2483	4.03	2.94	14.87	51.86	36.99	158.2
2483	4.03	2.79	14.87	51.86	36.99	156.3
2536	3.94	2.17	15.00	51.97	36.97	152.3
2591	3.86	1.89	15.13	52.09	36.96	152.3
					Avg.	155.7 $\pm$ 1.7

*fef reference temperature is 298°K.

TABLE 2 THE VAPORIZATION OF IRIDIUM IN THE PRESENCE OF CARBON

$1/T \times 10^4$ $°K^{-1}$	T $°K$	P_1 mm	$-\log_{10} P_{mm}$
4.29	2330	2.90×10^{-6}	5.54
4.18	2393	(A) 1.06×10^{-4}	3.98
4.11	2429	5.07×10^{-6}	5.30
4.05	2473	(B) 2.21×10^{-4}	3.66
4.05	2473	1.01×10^{-5}	5.00
4.03	2479	8.40×10^{-6}	5.08
4.03	2480	1.28×10^{-5}	4.89
3.97	2518	2.11×10^{-5}	4.68
3.95	2528	1.73×10^{-5}	4.76
3.94	2538	1.31×10^{-5}	4.88
3.91	2556	2.64×10^{-5}	4.58
3.88	2578	7.82×10^{-5}	4.11
3.83	2583	9.90×10^{-5}	4.00
3.83	2605	7.06×10^{-5}	4.15
3.80	2627	5.47×10^{-5}	4.26
3.79	2638	1.53×10^{-4}	3.81
3.79	2638	4.48×10^{-5}	4.35
3.76	2660	2.14×10^{-4}	3.67
3.72	2693	8.46×10^{-4}	3.07
3.64	2748	2.34×10^{-4}	3.63

X-ray studies of the residue remaining in the crucible after a run showed that only carbon and iridium were present. To study the platinum metal carbon systems more systematically, it will be necessary, either to do high temperature X-ray studies, or experiments in which the heated material is rapidly quenched and then analyzed.

C.   THE VAPORIZATION OF ALUMINA (Al_2O_3)

The data and the calculations for the study of the vaporization of Al_2O_3 are given in appendix C (a preprint of a note that has been prepared for publication). The preliminary data reported (ref. 1) for Al_2O_3 were found to be in error because of a malfunction of the integrating system in the mass spectrometer. This has been corrected for the work reported in appendix C.

D.   THE VAPORIZATION OF THORIA

Some preliminary studies of the vaporization of thoria have already been reported (ref. 1). The major species vaporizing from ThO_2 were stated to be $ThO_{2(g)}$, $ThO_{(g)}$, and $O_{(g)}$. It was assumed that the interaction of $ThO_{2(g)}$ with the electron beam to form ThO^+ ions was negligible.

Several mass spectrometric runs were undertaken to help determine the origin of the ThO^+ ions observed previously. Thoria and silica powders were heated to about $2300°K$ inside a thoria inner liner placed in a tungsten effusion cell. The cell was identical to that shown in figure 4, except that the iridium liner was omitted.

Since silica decomposes by the reaction,

$$SiO_{2(s)} \longrightarrow SiO_{(g)} + O_{(g)} \ , \tag{2}$$

it is possible by means of the above experiment to obtain a relatively high oxygen pressure within the effusion cell. In this case, the pressure of $O_{(g)}$ was observed mass spectrometrically to be approximately 50 times that of the $ThO_{2(g)}$. When 30 ev electrons were used, the ratio (R_1) of ion currents, $I_{ThO_2^+}/I_{ThO^+}$, due to ThO_2^+ and ThO^+ in the mass spectrometer, was found to be approximately 2.0 ± 0.3. Since it is presumed that in a strongly oxidizing atmosphere the equilibrium will be shifted in such a way that virtually all the thorium oxide species will be converted to $ThO_{2(g)}$, the ThO^+ ions observed in this experiment must have come from dissociative ionization of $ThO_{2(g)}$.

The effusion experiment with pure $ThO_{2(s)}$ was carried out in a nonoxidizing or reducing system at $2400°K$. An effusion cell with an iridium outer liner, identical to the tungsten outer liner shown in figure 22, was used. The ratio (R_2) of ion currents $I_{ThO_2^+}/I_{ThO^+}$ was found to be approximately between 1.5 and

2.0 . At $2300^\circ K$, R_2 was found to be about 1.0 ± 0.2 . The smaller value of the ratio, in this case, was presumably due to an increase in the relative amount of ThO^+ as a result of the effusion of $ThO_{(g)}$ from the cell.

Since under oxidizing conditions all the ThO^+ ions observed are presumed to be due to dissociative ionization of $ThO_{2(g)}$ by the electron beam, R_1 can be written as:

$$R_1 = \frac{P_{ThO_{2(eq)}} - KP_{ThO_{2(eq)}}}{KP_{ThO_{2(eq)}}} \quad , \tag{3}$$

where $P_{ThO_{2(eq)}}$ is the equilibrium pressure of $ThO_{2(g)}$ in the cell, and K is a constant equal to the fraction of the ThO_2 molecules undergoing dissociative ionization.

K is then solved as:

$$K = \frac{1}{R_1 + 1} \quad . \tag{4}$$

However, under neutral conditions, R_2 can be written as:

$$R_2 = \frac{P_{ThO_{2(eq)}} - KP_{ThO_{2(eq)}}}{P_{ThO_{(eq)}} + KP_{ThO_{2(eq)}}} = \frac{1 - K}{\frac{1}{R_{(eq)}} + K} \tag{5}$$

where $P_{ThO_{(eq)}}$ is the $ThO_{(g)}$ equilibrium pressure.

Finally, since the equilibrium ratio in a nonoxidizing atmosphere is expressed as:

$$R_{(eq)} = \frac{P_{ThO_{2(eq)}}}{P_{ThO_{(eq)}}} \quad , \tag{6}$$

it follows from the above relations that,

$$R_{(eq)} = \frac{R_2(R_1 + 1)}{R_1 - R_2} .$$
(7)

Then, if the appropriate values of R_1 and R_2 are substituted in equation (7), $R_{(eq)}$ (at $2300^\circ K$, neutral conditions) will be approximately 3. At $2400^\circ K$, if $R_1 = 2$, and $R_2 = 1.5$, then $R_{eq} \approx 9$. If under the same conditions $R_2 \approx 2$, then $(1/R_{eq})$ = $(ThO/ThO_2) = 0$, or $ThO = 0$, as assumed above. It thus appears that a process yielding $ThO_{(g)}$ may be significant in the vaporization of thoria.

Unfortunately, at the temperatures at which the experiments with ThO_2 could be carried out, the noise level in the mass spectrometer was very high and the signal to noise ratio very poor. In the work with ThO_2, a serious contribution to the noise level was presumed to occur from surface ionization of the ThO_2. Another reason was subsequent acceleration of the ions by the shielding of the electron bombardment furnace into the region of the mass spectrometer source end. Because of the high noise level, the limits of error of the ratios are uncertain. On the basis of the available evidence, the question of the importance of $ThO_{(g)}$ remains open and will bear further investigation.

If the sublimation reaction,

$$ThO_{2(s)} \longrightarrow ThO_{2(g)} ,$$
(8)

is considered independently, the slopes of the $\log I^+ T$ versus $1/T$ plots for $ThO_{2(g)}$ may be used to obtain an approximate heat of sublimation. Plots of the data obtained are given in figure 3. The lines were drawn with the aid of a least squares analysis of the points. The slopes of the least squares lines obtained for the runs in iridium lined cells and in tungsten cells yield heats of sublimation of approximately 145 and 167 kcal/mole , respectively. Statistical considerations of the data reveal that since there is a great deal of scatter in the data, difference between these values is not significant.

It is quite possible that some of the difficulties encountered in the study of the vaporization of ThO_2 arise from the fact that the stoichiometry of the evaporating solid changes. In this work, it has been observed that thoria sometimes loses an appreciable amount of oxygen when heated. It is therefore possible that the species observed in the various experiments result from the vaporization, not only from $ThO_{2(s)}$, but also from $ThO_{2-x(s)}$.

E.   THE VAPORIZATION OF HAFNIA

1.   Mass Spectrometric Studies

The vaporization of HfO_2 has been studied mass spectrometrically. The species effusing from unlined tungsten effusion cells, and from effusion
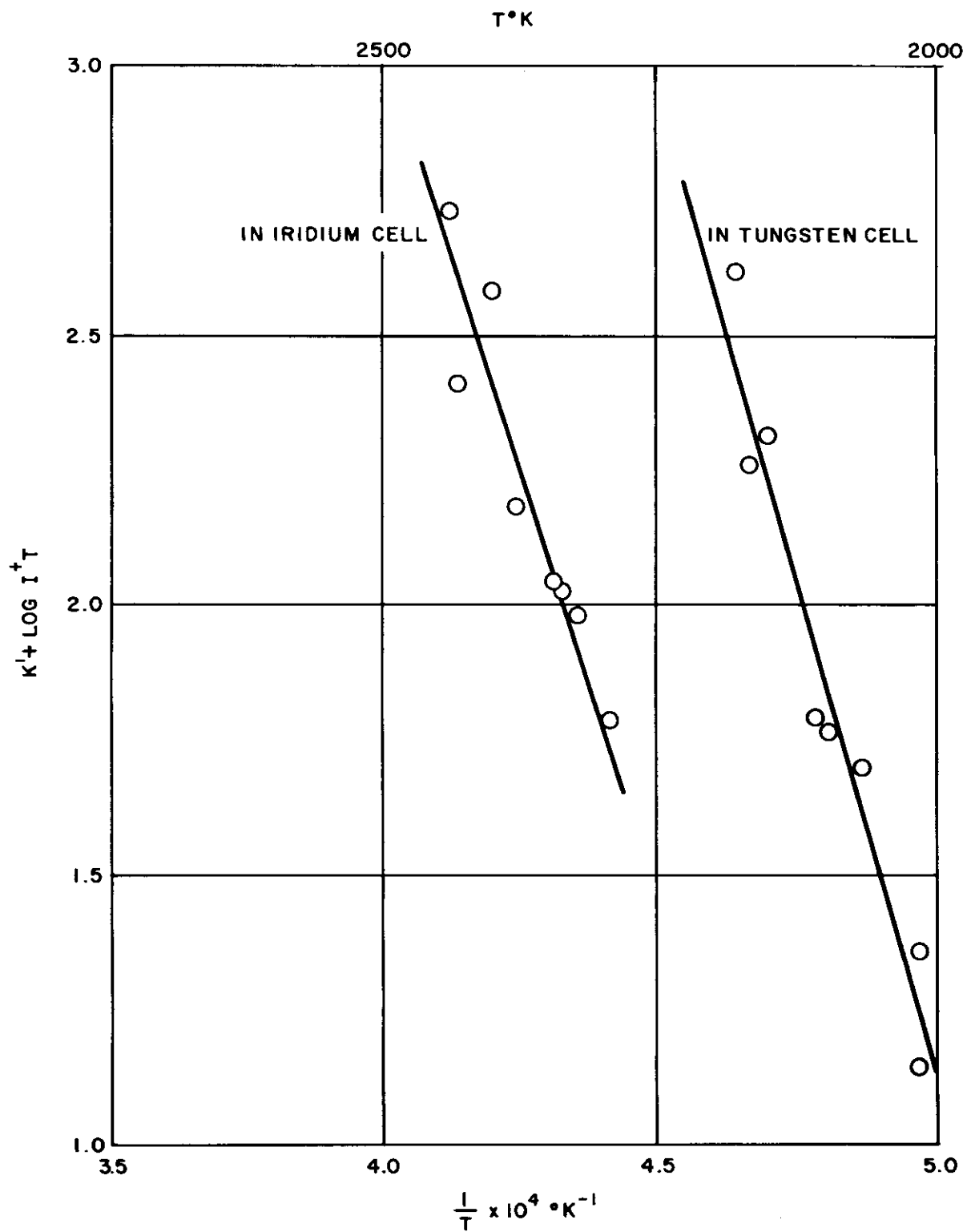
T°K

Figure 3 Log I⁺T versus 1/T for $ThO_{2(s)} \rightarrow ThO_{2(g)}$

cells containing thoria and iridium liners, were observed. The method of heating was the same as that described in appendix A. The effusion cell and liners were similar to those shown in figure 4. In all cases, the only ionic species containing hafnium (that resulted from the ionization of effusing species by 40, 25, and 17 volt electrons) were HfO^+ ions. O^+ ions could not be unambiguously observed because of a background peak at $m/e = 16$. When iridium and thoria liners were used, Ir^+_{191}, Ir^+_{193}, ThO^+, and ThO^+_2 were also observed.

It appears, on the basis of the mass spectrometric studies, that the observed HfO^+ ions arise from simple ionization of HfO molecules. The pressure in the system was much too low for ion-molecule combination to have been significant. Then, if dissociative ionization from a higher molecular-weight species had occurred, it is probable that enough simple ionization would have existed for the species to have been detected. No ions of higher molecular weight containing hafnium were observed.

2. Stoichiometric Studies

After the work described above, and the simple effusion studies described below were completed, examination of the residue left in the cell after a run revealed that the hafnia had turned gray.

Studies were undertaken to determine what changes occur in the condensed phase when hafnia is vaporized. Samples of spectroscopic grade hafnia were heated in tungsten and iridium crucibles to temperatures in the range from 2300° to 2600°K in vacuum, for various lengths of time. The samples that were heated in the tungsten container appeared to turn a uniform gray. Those in iridium appeared to consist of white and dark phases. When these samples were reheated in air, they turned white again and showed a small weight gain. The samples of oxygen poor material originally heated in tungsten corresponded then to an average composition of $HfO_{1.997 \pm .001}$, if it is assumed that the white material was $HfO_{2.000}$. The sample originally heated in iridium lost considerably less oxygen.

A microscopic inspection revealed that in both cases the sample remaining after heating consisted of a thin layer of dark material, over a much greater mass of the white starting material.

X-ray studies revealed that the white material was the starting monoclinic phase of HfO_2. The darker phase was found to be cubic, but only a very small amount of the material was obtained, and no further detailed studies could be made.
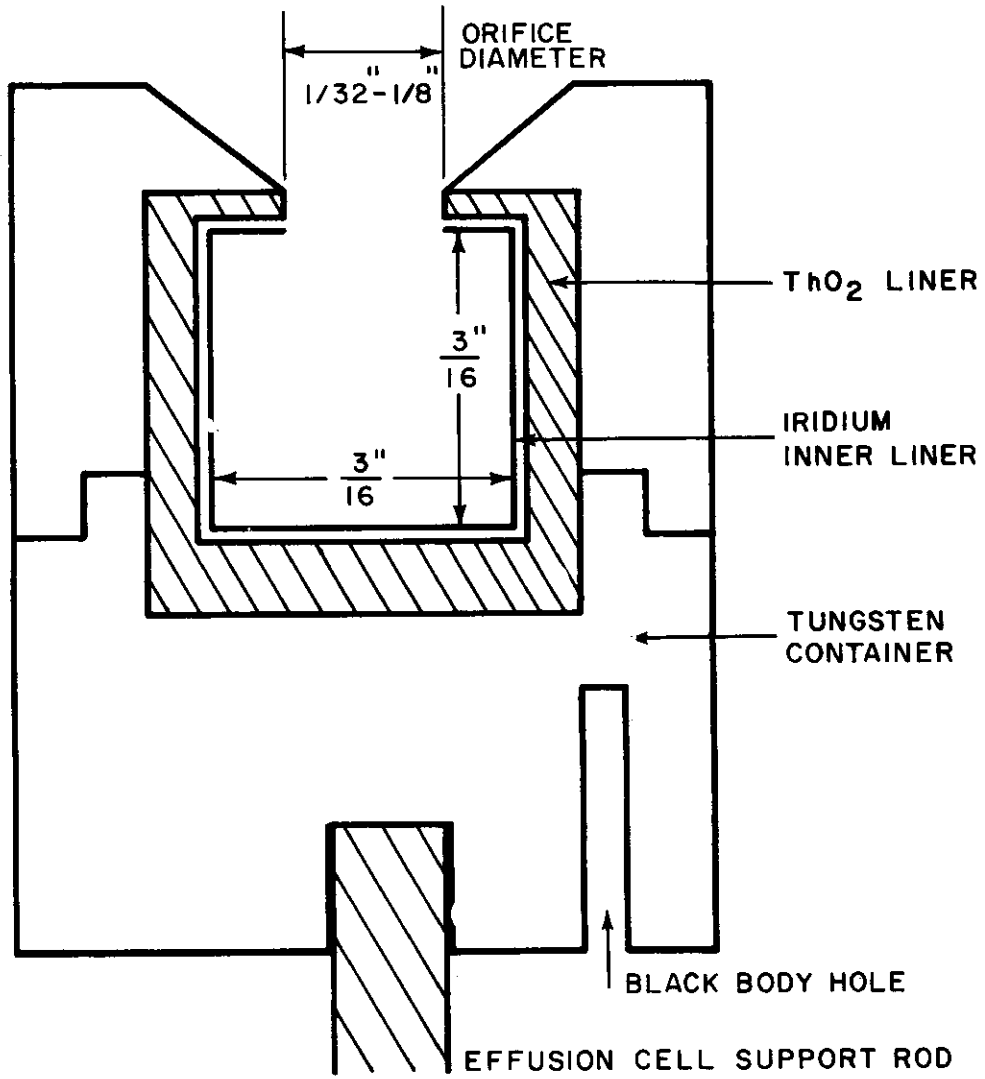
ORIFICE
DIAMETER

1/32"−1/8"

3"/16

3"/16

ThO$_2$ LINER

IRIDIUM
INNER LINER

TUNGSTEN
CONTAINER

BLACK BODY HOLE

EFFUSION CELL SUPPORT ROD

Figure 4 The effusion cell

3. Simple Effusion Studies

Simple effusion studies were undertaken in which hafnia, containing Hf^{181} as a tracer, was vaporized from effusion cells with iridium liners. The material used in these studies was taken from a standard reactor irradiated unit of HfO_2 , obtained from Oak Ridge National Laboratory. The effusion cell, used in the initial work, consisted of a relatively massive outer tungsten shell, a thin thoria separator, and an iridium inner liner. The cell is illustrated in figure 4 . Orifice diameters of approximately 1/16 and 1/32 in. were used, and a collimated portion of the effusion beam was caused to impinge upon copper targets, cooled with liquid nitrogen. The apparatus and procedures were essentially the same as those described for the rhodium and iridium studies.

The amount of Hf assumed to be deposited as HfO upon the target was found by determining the radioactivity of the target. This was compared to the radioactivity of a calibrated sample, containing a known amount of Hf with the same ratio of Hf^{181} to normal Hf , as the sample in the effusion cell. The calibrated sample was a small quantity of the starting material in solution. The solution was obtained by dissolving a weighed portion of the HfO_2 in warm concentrated HF , adding concentrated H_2SO_4 , fuming off the HF, diluting to the required volume, and taking an aliquot as a standard.

The initial data were found to be very scattered. Inspection after the runs revealed that the iridium cells were severely attacked in some instances, apparently from the outside. This may have been caused by alloying with thorium metal, formed from the interaction of thoria and tungsten. Where the iridium cell had been punctured, the thoria liner was highly contaminated with Hf^{181} . Where there was no puncture no activity of Hf^{181} was observed outside the iridium liner.

In an effort to eliminate the disturbing side reaction effects of iridium with the presumed products of the thoria-tungsten reaction, effusion studies were done where the thoria separator (see figure 4) was replaced by a packing of powdered hafnia. In this case, the iridium liner no longer was attacked, and it was possible to retain all the points of a given run.

The data then obtained were scattered in a similar manner to the data discussed above, except that the pressures obtained were somewhat higher. In these studies, iridium effusion cell liners with 1/32 in. orifices were used. It appears, on the basis of the observations in the stoichiometry studies, that there was some formation of a phase (or phases) of HfO_{2-x} on the surface of the HfO_2.

It appeared that the calculated pressures at the start of a run were higher than those at the end, at a given temperature. This did not always occur,

however, as the thin coating of the new phase probably did not remain coherent during a run. The data for these experiments are shown in figure 5. The upper solid line represents an estimated upper limit for the data, and if the assumptions made above are correct, represents approximately, the vapor pressure of HfO from the reaction,

$$HfO_{2(s)} \longrightarrow HfO_{(g)} + O_{(g)} \ . \qquad (9)$$

The lower line, if it is due to a single phase in equilibrium with the gas, represents the $\log p$ versus $1/T$ curve for the process,

$$HfO_{2-x(s)} \longrightarrow HfO_{(g)} + (1-x)O_{(g)} \ . \qquad (10)$$

The ΔH_{298} values for these reactions were found to be 347 and 357 kcal/mole , respectively. They were obtained from third law calculations with free energy functions, tabulated by Brewer (ref. 3,4), and Stull and Sinke (ref. 2). It was assumed that x was small and the free energy function for $HfO_{2(s)}$ was the same as that for $HfO_{2-x(s)}$. The individual data points were not used in these calculations. Several points were selected instead from the upper and lower lines. The data for these studies are given in Table 3.

F.   THE VAPORIZATION OF THE RARE EARTH SESQUIOXIDES

A mass spectroscopic survey of the vaporization mode of the rare earth oxides was undertaken. The results of the survey, with the exception of the work with CeO_2 and Ce_2O_3 , are given in appendices D and E that have been prepared for publication.

Preliminary studies of the vaporization of the cerium oxides indicated that $CeO_{2(s)}$ vaporizes principally as $CeO_{2(g)}$, and that $Ce_2O_{3(s)}$ vaporizes principally to yield $CeO_{(g)}$ with appreciable amounts of $CeO_{2(g)}$. No Ce vapor was observed. Not enough work has been done on cerium oxide to determine whether the $CeO_{2(g)}$ from the sesquioxide vaporization arises from actual vaporization of Ce_2O_3 , or from some residual CeO_2 present in the sample.

G.   CONTINUOUSLY MONITORED EFFUSION EXPERIMENTS

At the present time, for all practical purposes, rocket nozzle materials are being selected by means of a purely intuitive approach. It is generally thought that materials which melt at very high temperatures have the most promise of proving to be satisfactory nozzle materials. The futility of this approach has been demonstrated on many occasions. Part of the explanation for the continued existence of these selection methods rests on the lack of sufficient thermodynamic data on which to base a sounder theoretical approach. Therefore, to
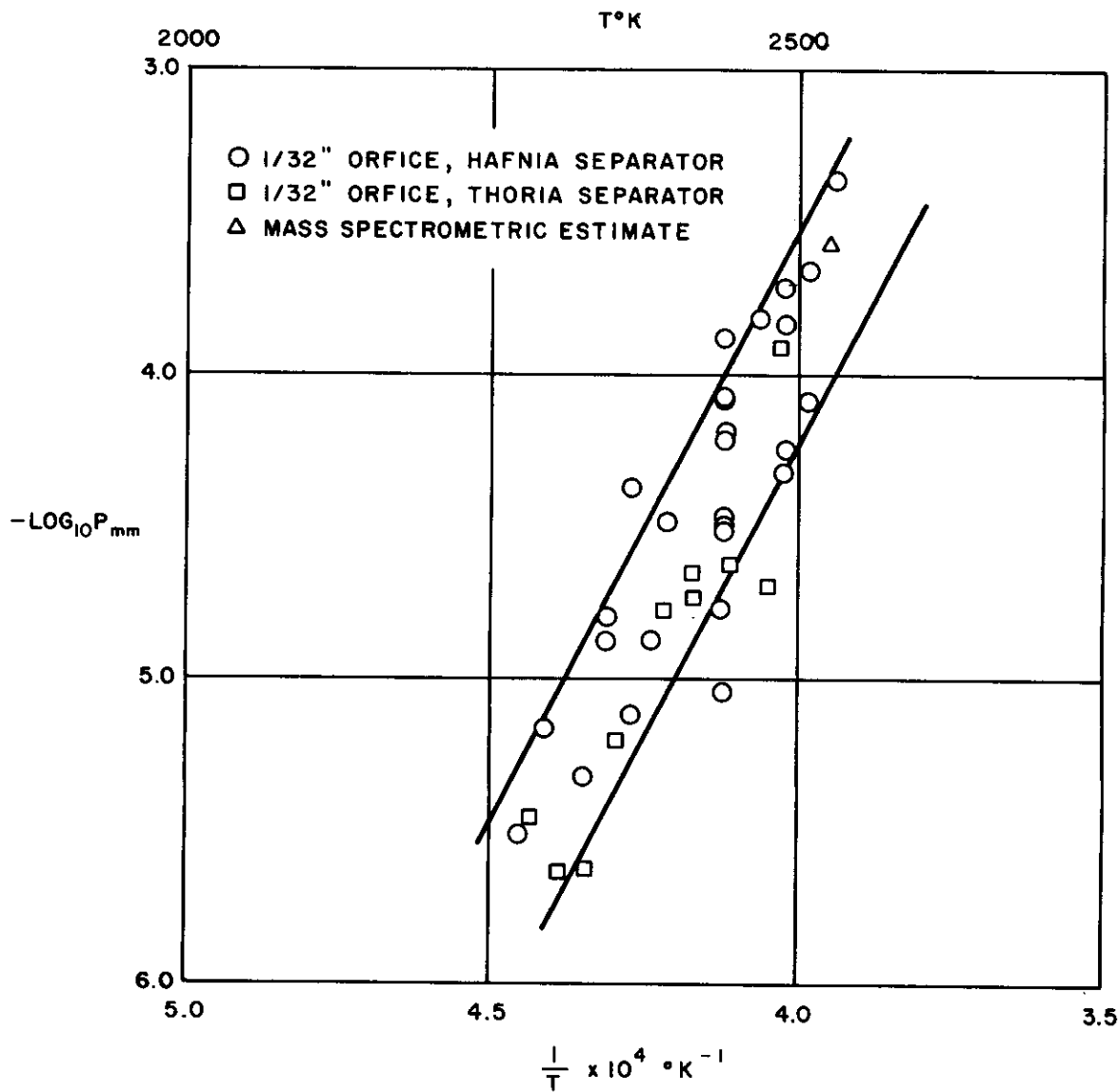
Figure 5 Log P versus 1/T for $HfO_{(g)}$ from $HfO_{2(s)}$

TABLE 3 THE VAPORIZATION OF HAFNIA (HfO_2)

T $°K$	$-\log_{10}P_{mm}$ (HfO)	Separator*	T $°K$	$-\log_{10}P_{mm}$ (HfO)	Separator*
2246	5.51	HfO_2	2429	4.47	HfO_2
2254	5.54	ThO_2	2429	4.50	HfO_2
2268	5.17	HfO_2	2429	4.47	HfO_2
2276	5.63	ThO_2	2429	4.51	HfO_2
2300	5.32	HfO_2	2429	4.77	HfO_2
2322	4.79	HfO_2	2429	4.20	HfO_2
2322	4.80	HfO_2	2429	4.08	HfO_2
2330	5.21	ThO_2	2429	4.09	HfO_2
2343	5.12	HfO_2	2429	4.22	HfO_2
2343	4.38	HfO_2	2461	3.83	HfO_2
2356	4.89	HfO_2	2471	4.70	ThO_2
2373	4.77	ThO_2	2482	3.91	ThO_2
2375	4.49	HfO_2	2483	3.84	HfO_2
2395	4.72	ThO_2	2483	4.25	HfO_2
2400	4.65	ThO_2	2483	3.72	HfO_2
2427	4.63	ThO_2	2483	4.32	HfO_2
2429	4.21	HfO_2	2515	3.67	HfO_2
2429	5.04	HfO_2	2515	4.09	HfO_2
2429	3.89	HfO_2	2536	3.37	HfO_2
2429	4.45	HfO_2			

* The material used to separate the iridium inner liner from the tungsten outer liner.

help accumulate such thermodynamic data at an accelerated pace, a modified evaporation technique has been developed. This technique determines the thermodynamic properties of the systems of interest to the designers of solid-fuel propelled rocket nozzles.

A discussion of continuously monitored effusion experiments is included in appendix F. The apparatus used for these experiments has been described previously (ref. 1). The systems that have been investigated by this technique are: 1) The molybdenum-silicon system, 2) The tungsten-silicon system, and 3) The tantalum-boron system.

1. Molybdenum-Silicon System

The molybdenum-silicon system is of interest to those concerned with materials of construction, mainly because of the known high temperature oxidation resistance of some of its phases (ref. 5). A phase diagram of the system is shown in figure 6. In compiling this phase diagram, the melting points given by Hansen (ref. 6), the stoichiometry of Mo_3Si and $MoSi_2$ given by Hansen (ref. 6), and the stoichiometry of Mo_5Si_3 given by Aronsson (ref. 7), were used. These were considered reliable enough to allow the major emphasis in these experiments to be placed upon the determination of the pressures of silicon above the various equilibrium condensed phases of the system.

Several experimental techniques were investigated for the molybdenum-silicon system. The experimental methods that were attempted can be divided into three groups:

a. Those experiments in which silicon was effused from various mole ratios of molybdenum and silicon powders while the powders were interacting in molybdenum or tungsten effusion cells.

b. Those experiments in which silicon was effused from prereacted compositions of molybdenum and silicon (e.g., $MoSi_2$) in tungsten or molybdenum crucibles.

c. Those experiments in which silicon was effused from a molybdenum crucible in which silicon powder had been placed.

It is important to note that in interpreting the results of a continuously monitored effusion experiment, it is assumed that all concentration gradients occur in a direction perpendicular to the evaporating surface. In these cases where powders are used, it is assumed that the evaporating surface is the upper surface of the particles taken as a whole and not the surface of the individual particles (i.e., at any given depth from the surface of the powder bed the concentration is constant).
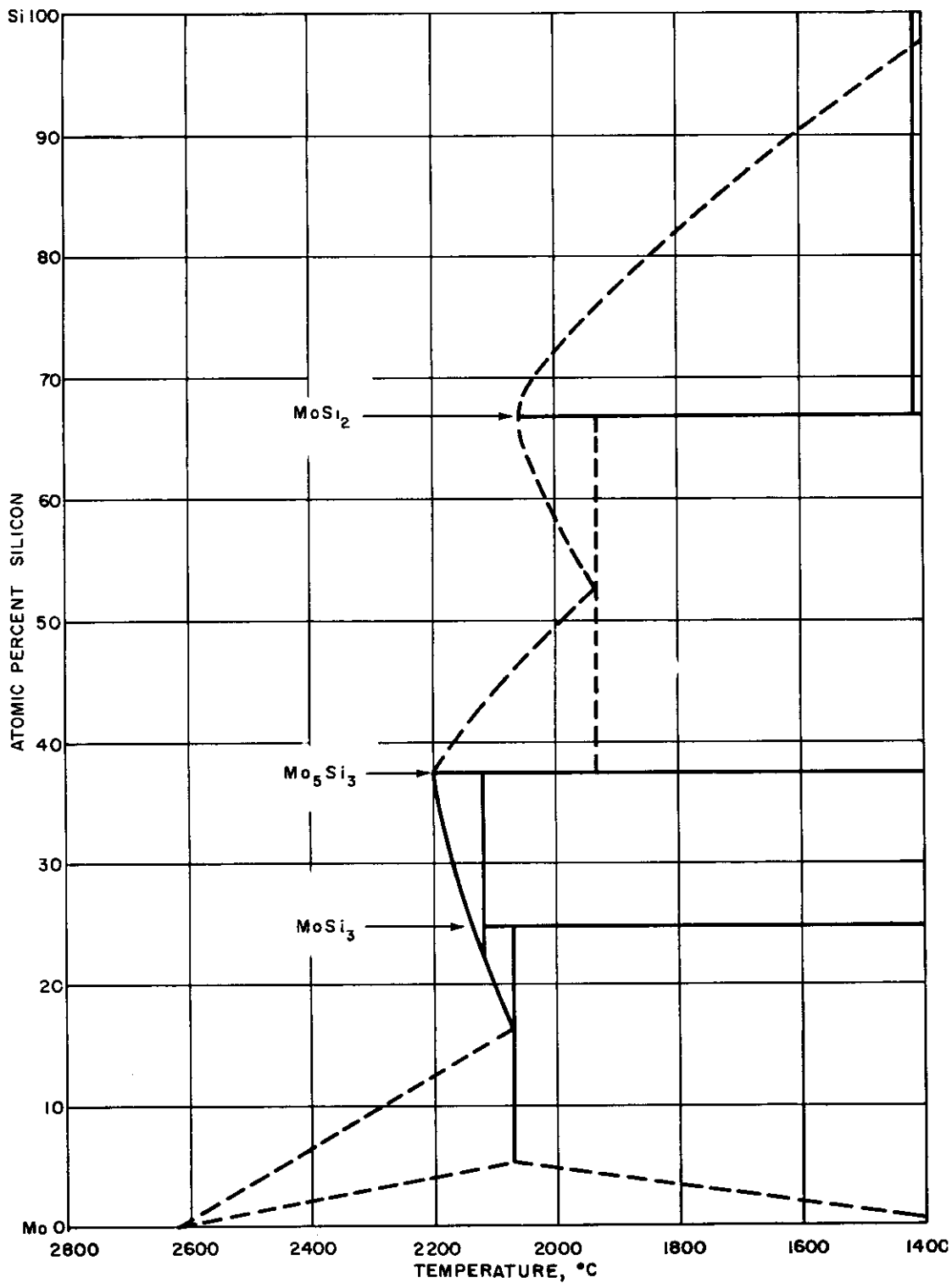
Figure 6 Phase diagram of the molybdenum - silicon system

Optical and X-ray examination in many cases where the first two methods were used, indicated that what was assumed to be the evaporating surface was not single phase, but consisted of noncompatible phases, according to the phase diagram, e.g., mixtures of $MoSi_2$, Mo_5Si_3 , and Mo_3Si . The results of those cases where there appeared to be appreciable surface non-uniformity were not used.

The most reliable results were obtained from the third method, that of effusion of silicon from a molybdenum crucible. The silicon apparently formed a liquid phase at the beginning of the experiment. The measured vapor pressure decreased continuously, indicating that a solution or compound of lower silicon activity was being formed.

The actual experimental technique involved placing 20 to 200 milligrams of powder in a crucible of the dimensions shown in figure 7 and continuously monitoring the isothermal rate of evaporation of silicon from this system by techniques previously described (ref. 1).

The volatility of the silicon in the various regions of the graphs (shown in figures 8 through 12) may be interpreted as follows:

a.   There is an initial region that exhibits a decreasing volatility, interpreted as being due to the interaction and dissolution of molybdenum in silicon.

b.   Also, there is a second region, assumed to be due to the evaporation of silicon from the two-phase region of the phase diagram containing liquid silicon (of the molybdenum concentration prescribed by the phase diagram), and $MoSi_2$.

c.   The subsequent regions of the volatility curves are assumed to correspond to two-phase regions containing $MoSi_2 - Mo_5Si_3$, $Mo_5Si_3 - Mo_3Si$, and $Mo_3Si - Mo$, respectively.

The vapor species above the various molybdenum-silicon compositions have been determined to be monomeric silicon by means of a Bendix time-of-flight mass spectrometer.

One of the serious sources of error in these experiments was the control and measurement of temperature. All attempts to sight an optical pyrometer directly on the sample, or to sight it on a hole in the crucible, proved unreliable. An attempt will be made to redesign the furnace to automatically control and record the power to the furnace and also, to determine the relation between temperature and power fed into the furnace. This relation will be determined in two ways (1) Comparison of the power input with
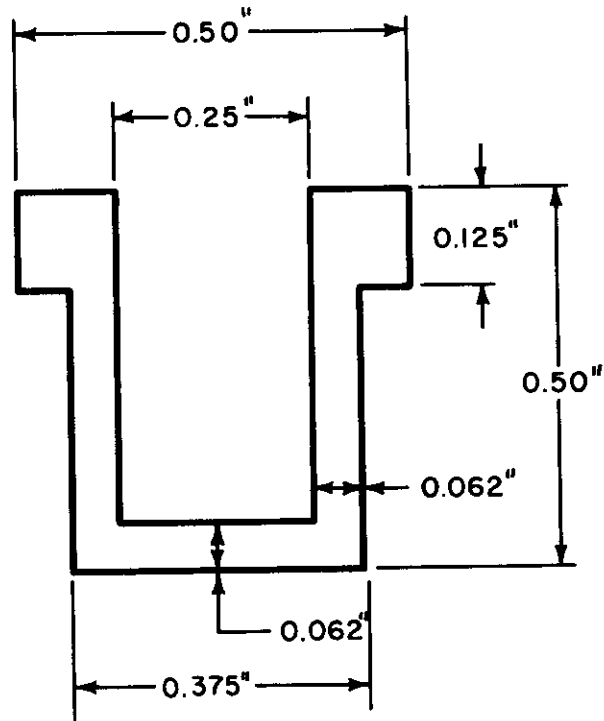
Figure 7 Crucible shape for silicon evaporation experiments
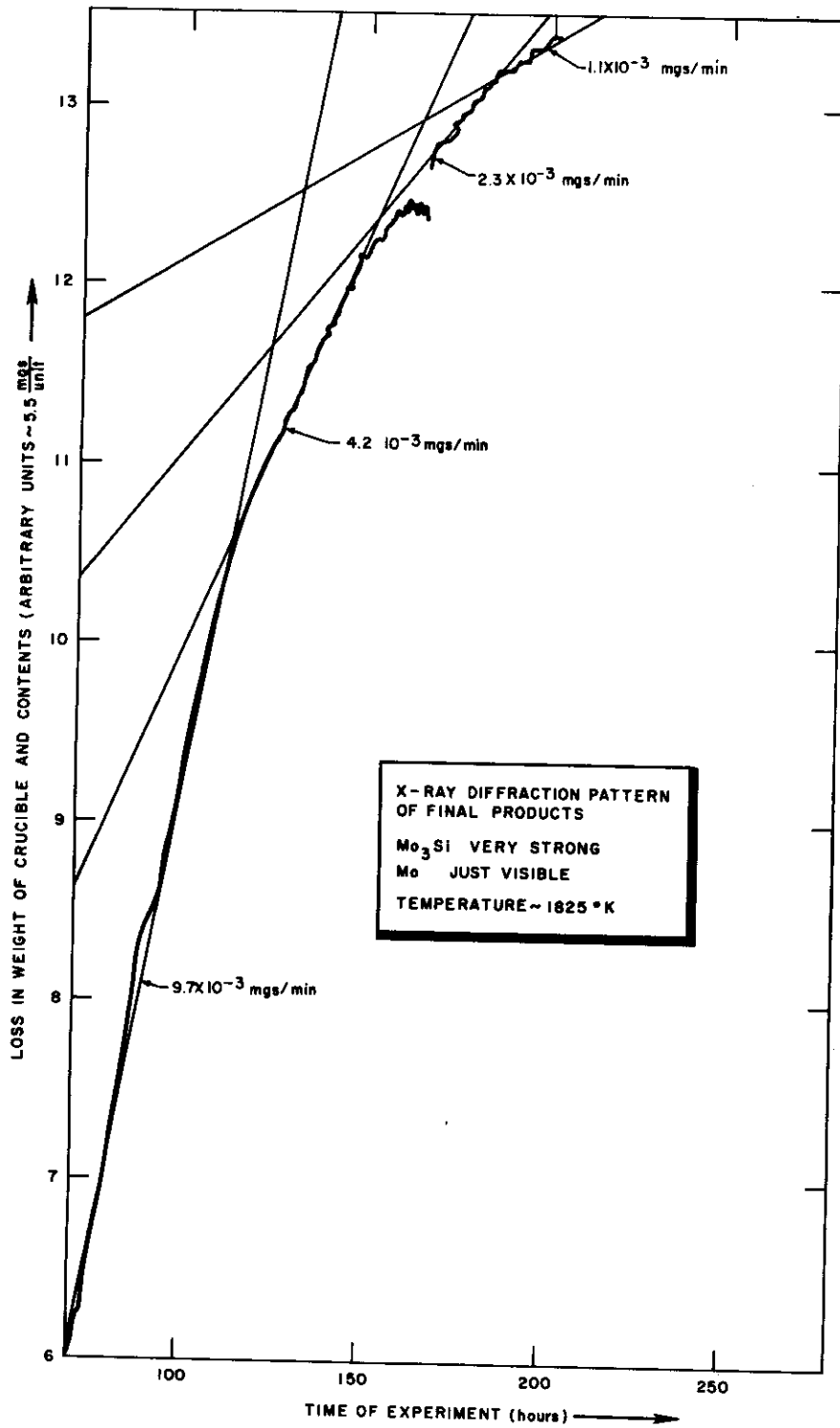
Figure 8   Evaporation of silicon from a molybdenum crucible at 1825°K

Figure 9 Evaporation of silicon from an equal weight mixture of silicon, and molybdenum powders, in a tungsten crucible, at 1760°K

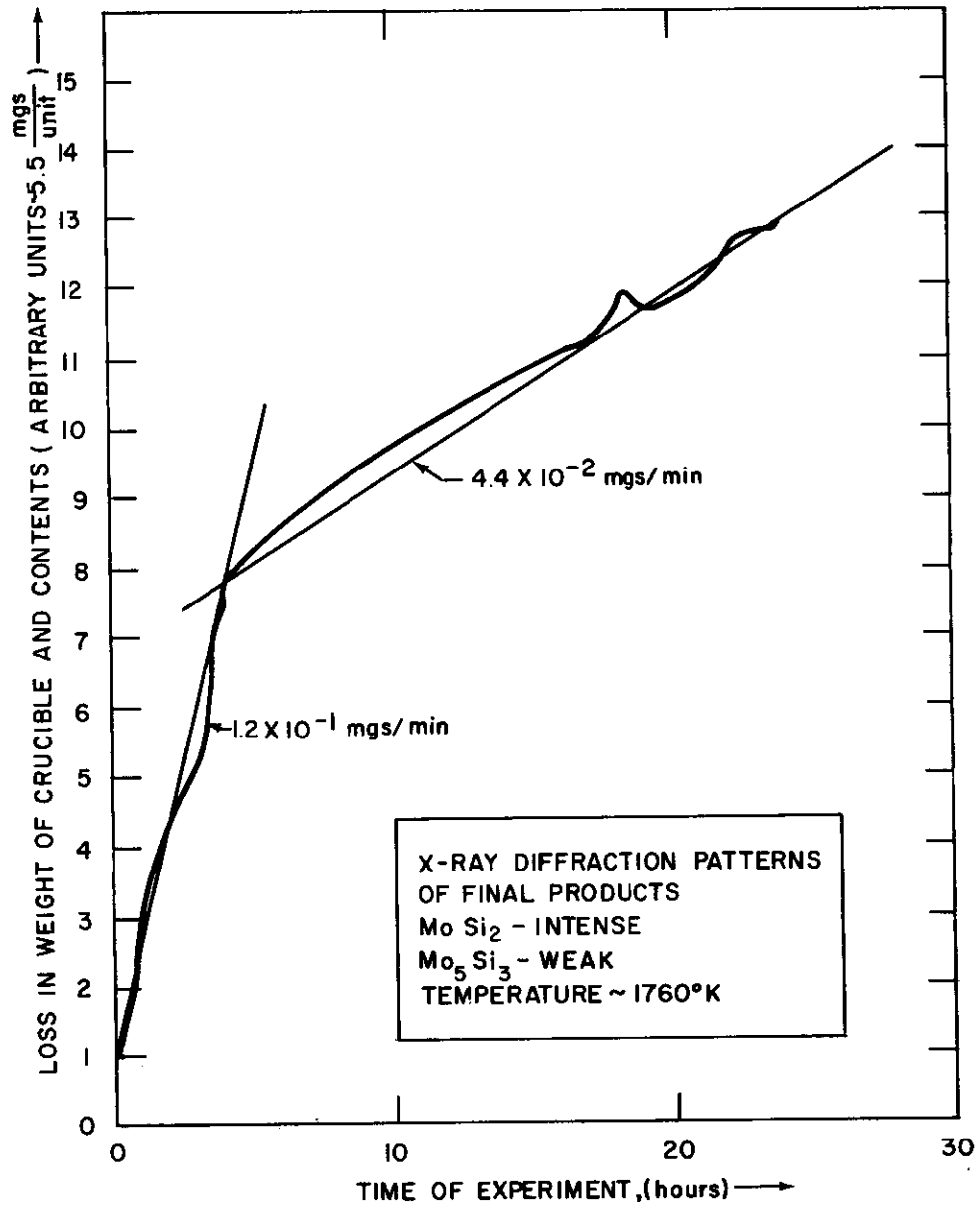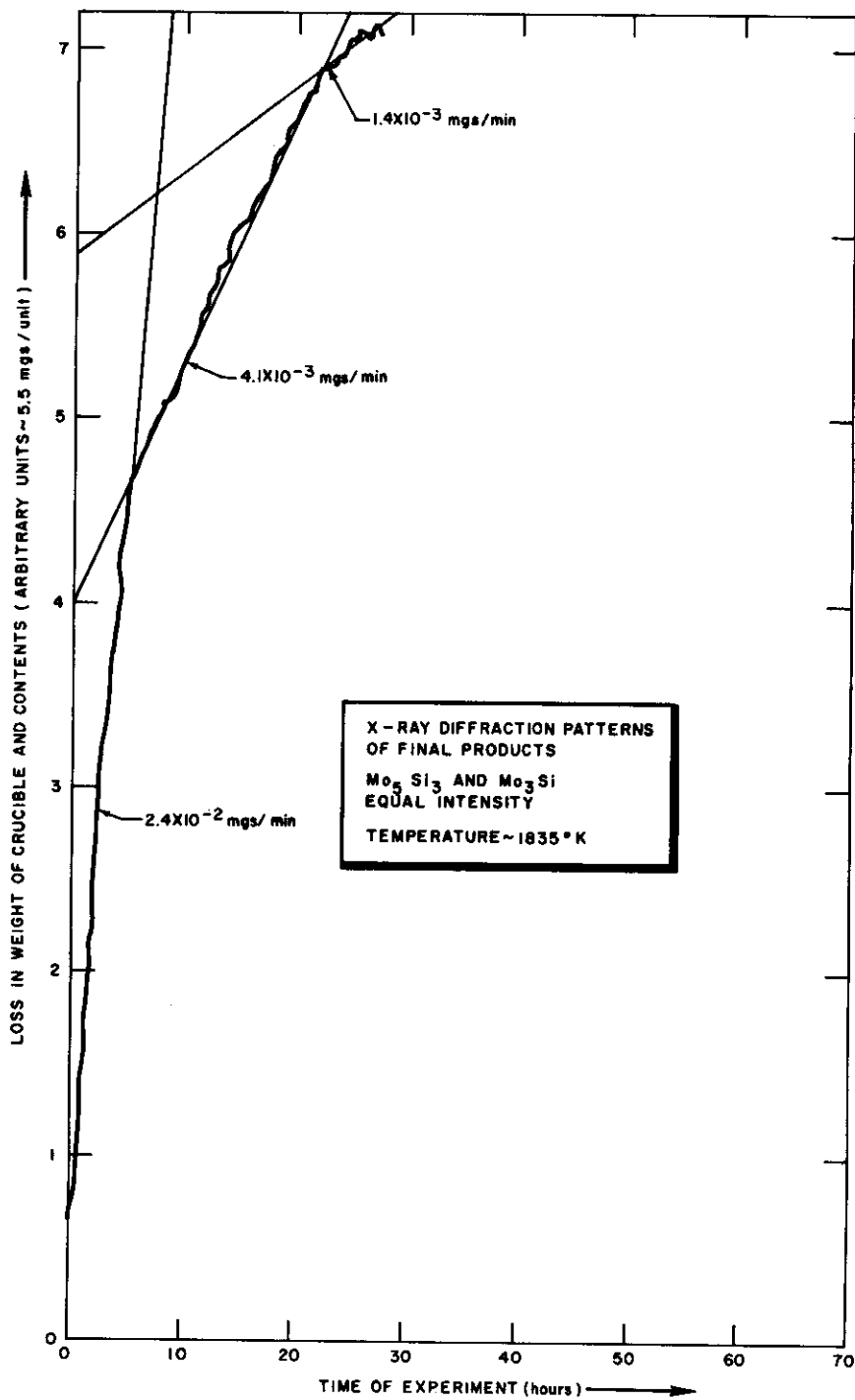Figure 10 Evaporation of silicon from an equal weight mixture of silicon, and molybdenum powders, in a molybdenum crucible, at 1835°K
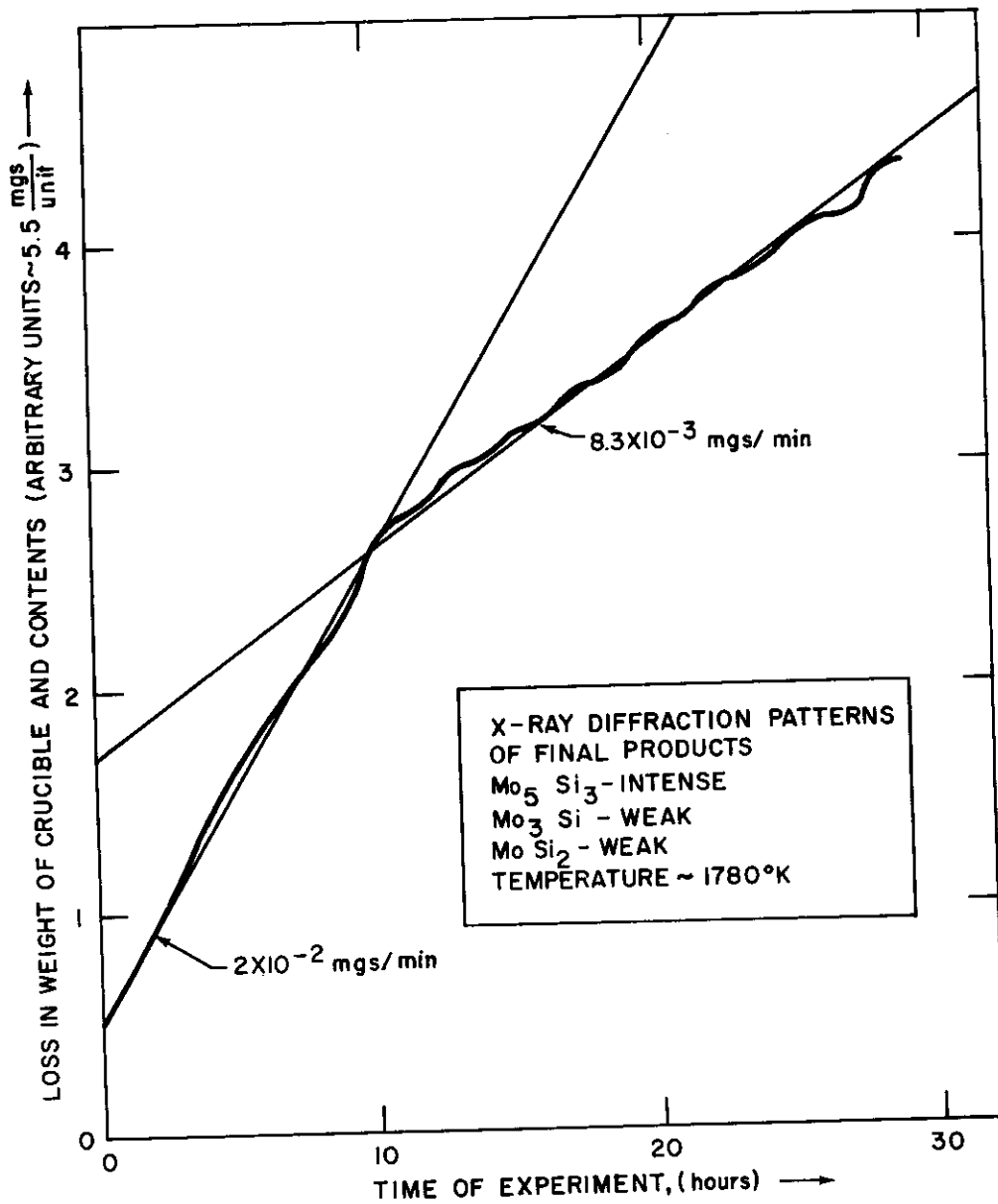
Figure 11 Evaporation of silicon from a mixture of silicon and molybdenum in the atomic ratio Mo:2Si , in a tungsten crucible, at 1780°K

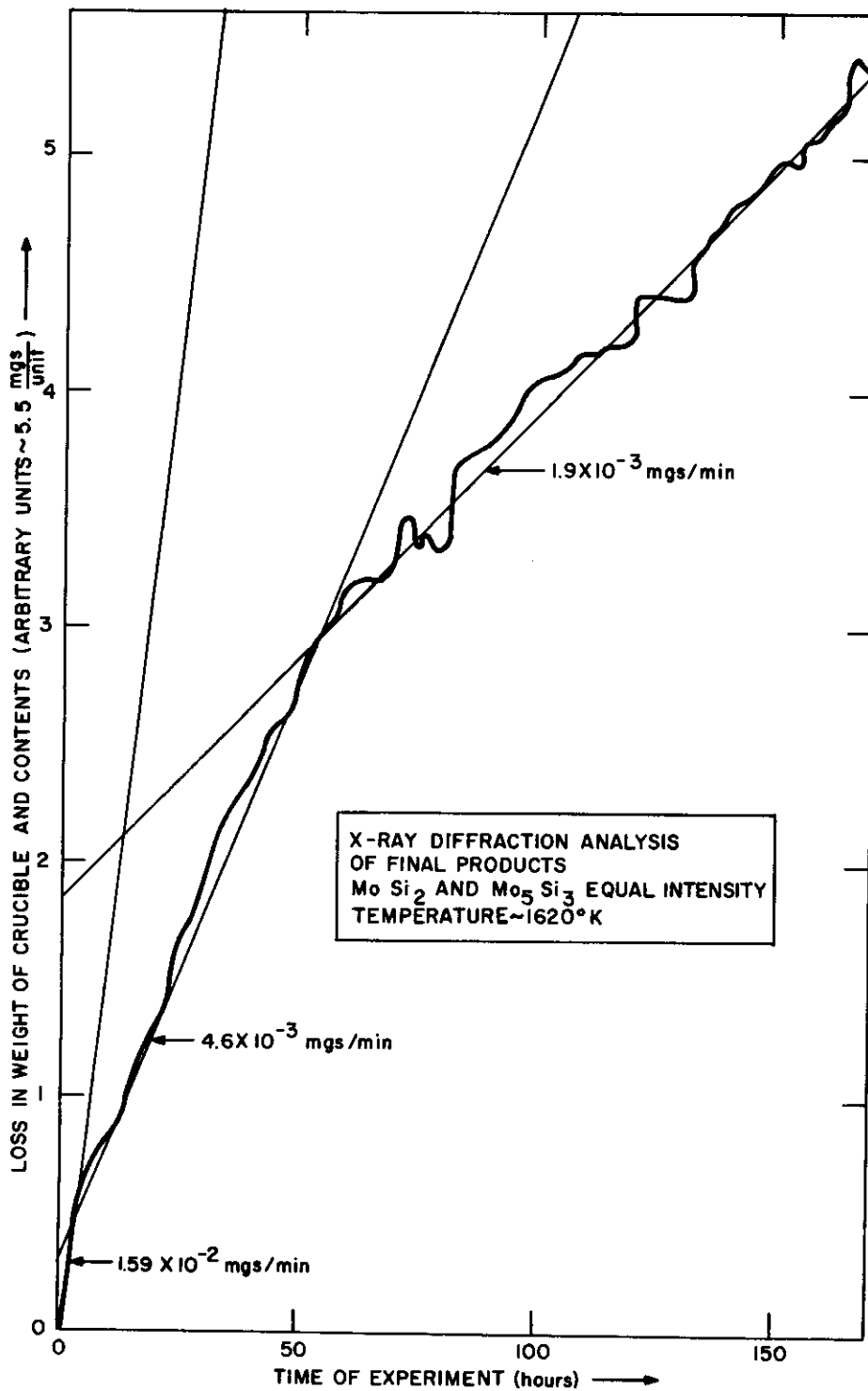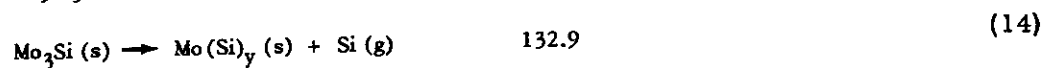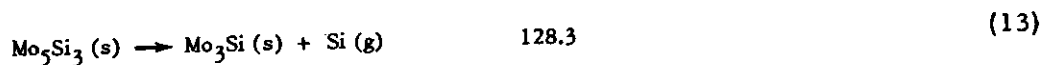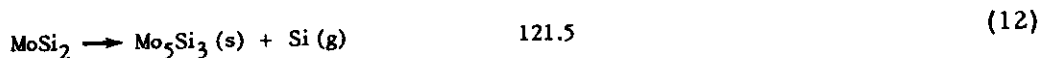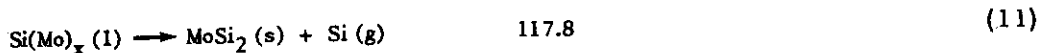Figure 12 Evaporation of silicon from an equal weight mixture of
molybdenum and silicon powders, in a tungsten crucible,
at 1620°K

thermocouple readings and, (2) Comparison of the power input with the rates of evaporation of elements, whose rates of evaporation as a function of temperature are well known.

A third law calculation of the results of this investigation uses the values of the free energy functions $(\Delta F_T - \Delta H_{298})/T$ of $MoSi_2$, Mo_5Si_3, and Mo_3Si, given by Searcy and Tharp (ref. 8). The heats of dissociation in kilocalories per gram atom of silicon at 298°K are:

$$Si(Mo)_x (l) \longrightarrow MoSi_2 (s) + Si (g) \qquad 117.8 \qquad\qquad (11)$$

$$MoSi_2 \longrightarrow Mo_5Si_3 (s) + Si (g) \qquad 121.5 \qquad\qquad (12)$$

$$Mo_5Si_3 (s) \longrightarrow Mo_3Si (s) + Si (g) \qquad 128.3 \qquad\qquad (13)$$

$$Mo_3Si (s) \longrightarrow Mo(Si)_y (s) + Si (g) \qquad 132.9 \qquad\qquad (14)$$

It is estimated that at the present time an error of at least ± 6 kcal/g-atom Si must be associated with the results of this experiment.

While this investigation was in progress, Searcy and Tharp (ref. 8) published the results of the dissociation pressures of the molybdenum silicides. The following heats of dissociation in kilocalories per gram atom of silicon at 298°K were reported:

$MoSi_2$, 117.2; Mo_5Si_3, 131.1; and Mo_3Si, 131.9.

The results of this investigation cannot be meaningfully compared with those obtained by Searcy and Tharp until certain questions concerning the steady state surface compositions and temperature of the specimens used in the present investigation have been resolved.

2. Tungsten-Silicon System

Studies similar to those of the molybdenum-silicon system have been conducted for the tungsten-silicon system by measuring the isothermal rate of evaporation of silicon from tungsten crucibles. A phase diagram of the W-Si system (ref. 9) is shown in figure 13. The results of such an experiment are shown in figure 14. The same difficulties concerning equilibrium and temperature measurement have been encountered in this system as in the molybdenum-silicon system.

WADD TR 60-463 Pt. II
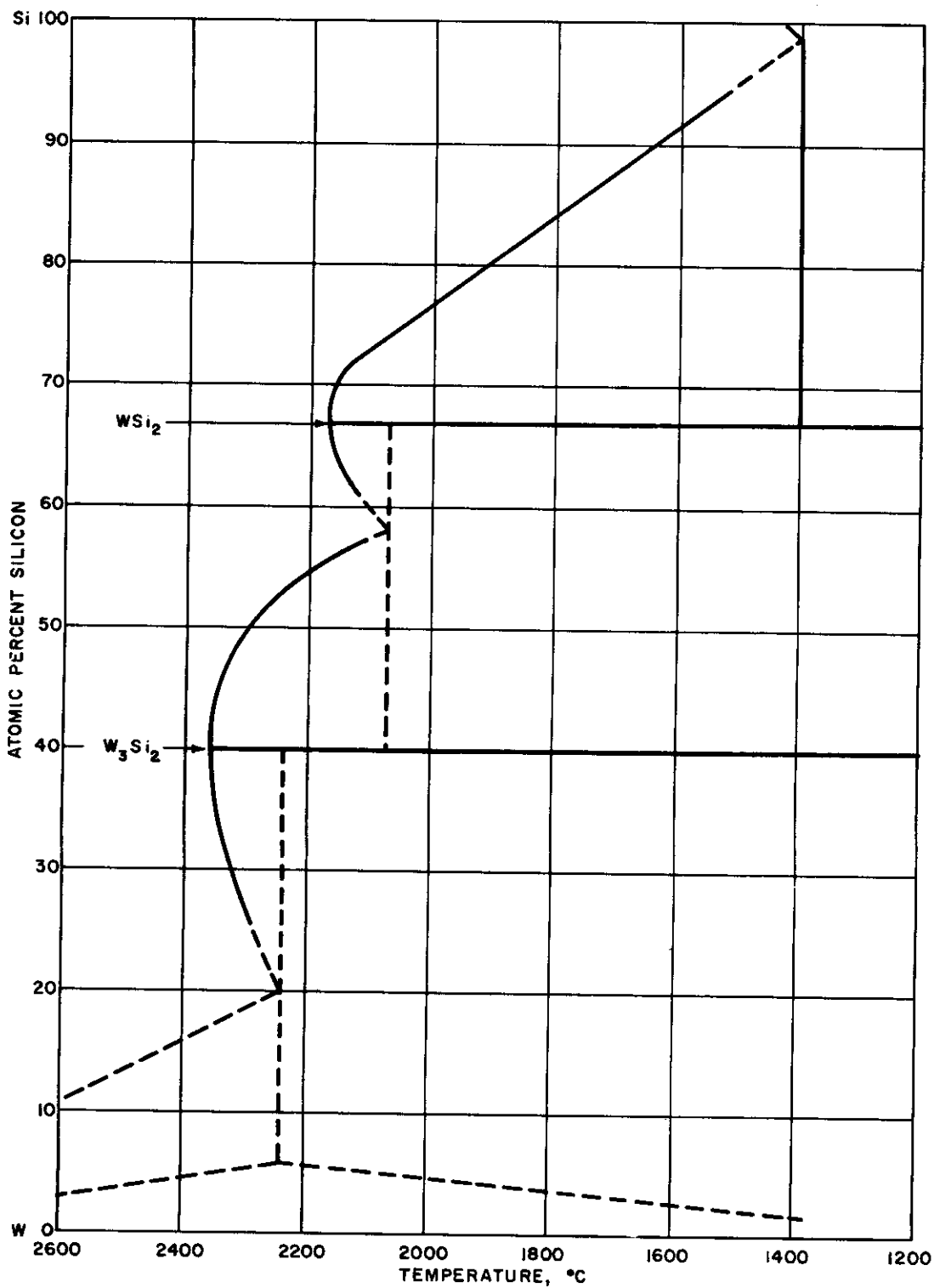
Figure 13 Phase diagram of the tungsten - silicon system
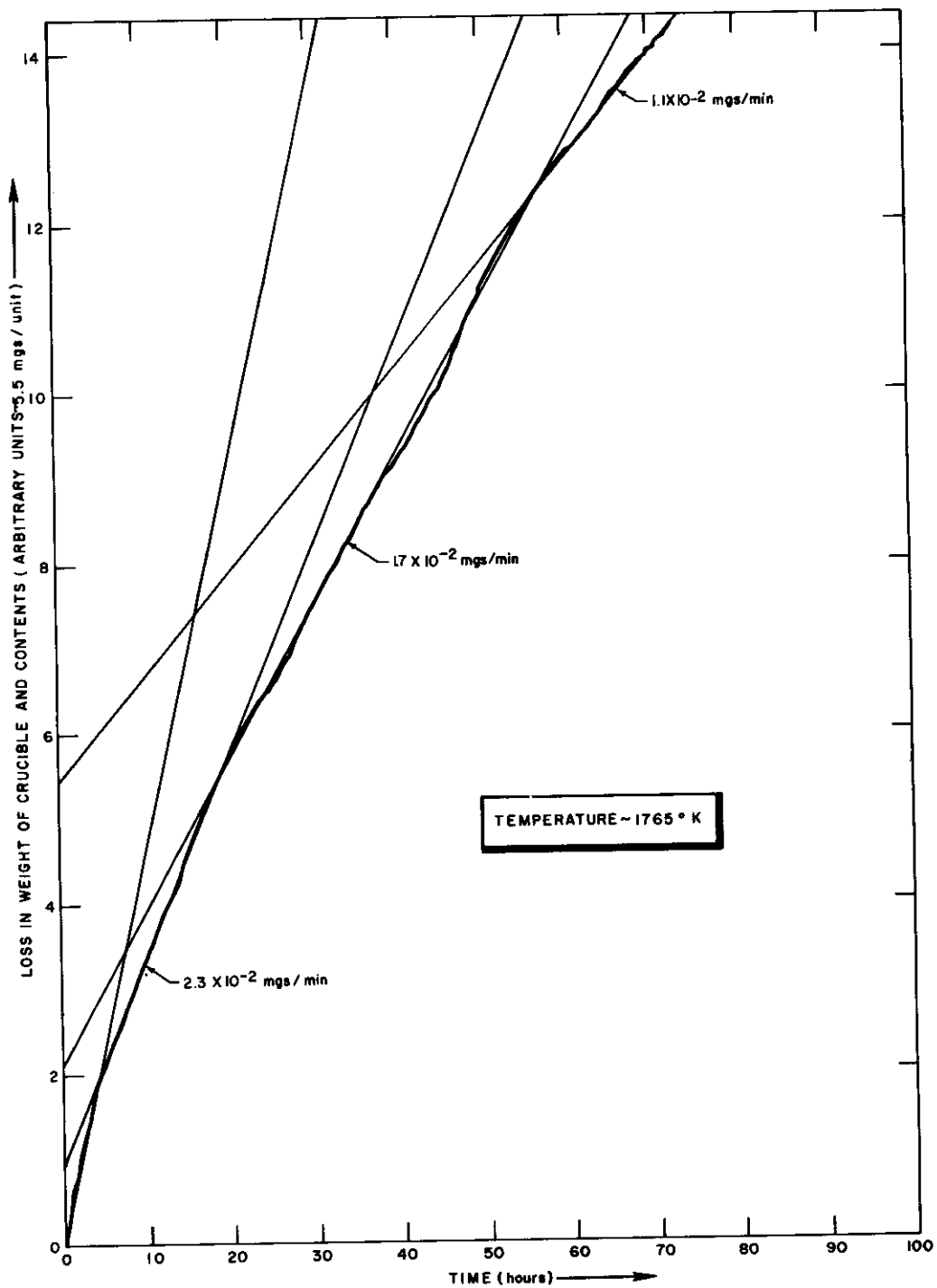
Figure 14 Evaporation of silicon from a tungsten crucible

At 1765°K, the following dissociation pressures of silicon were obtained for this system:

$$Si\ (W)_x \longrightarrow WSi_2 + Si\ (g)\quad 3.5 \times 10^{-6}\ atm, \tag{15}$$

$$WSi_2 \longrightarrow W_3Si_2 + Si\ (g)\quad 2.6 \times 10^{-6}\ atm,\ and \tag{16}$$

$$W_3Si_2 \longrightarrow W(Si)_y + Si\ (g)\quad 1.7 \times 10^{-6}\ atm. \tag{17}$$
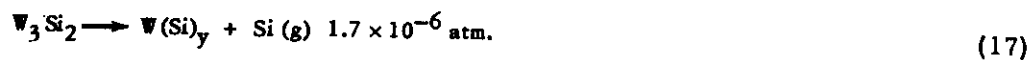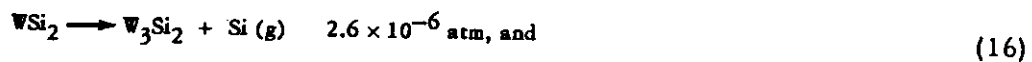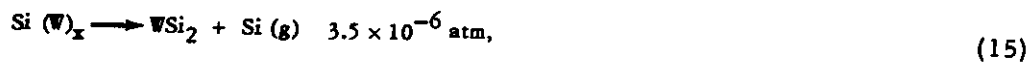
3.   Tantalum-Boron System

Serious difficulties have been encountered in obtaining continuously monitored effusion data of the tantalum boron system.

The experiments where boron was evaporated from a tantalum crucible showed the final products to be boron powder and a coating of a tantalum boride on the crucible wall. In the experiments where the evaporation of boron was monitored from a reacting mixture of tantalum and boron powders, the final products were mixtures of Ta, TaB_2, Ta_3B_4 and TaB.

The measurement of the isothermal rate of evaporation of boron from dense coatings of tantalum boride on the inside of a tantalum crucible (ref. 10) should enable the dissociation pressures of the tantalum boron system to be measured.

II. SURFACE TENSION STUDIES

The surface tensions of various refractories have been determined by a sessile drop technique (refs. 11, 12). The maximum diameter and height of the apex of the drop above the maximum diameter were measured in the apparatus shown in figure 15. These quantities were substituted into the equations of Bashforth and Adams (ref. 13) to obtain the requisite surface tensions. The apparatus used in these experiments consisted of an outer quartz envelope, an inner opaque quartz heat shield, and an inductively heated tantalum susceptor, supported by boron nitride end pieces.

The application of the Bashforth and Adams equations to drops formed on a flat plate is limited to those materials forming drops with obtuse contact angles. However, all of the materials tested under this program wet their substrates.

To circumvent this difficulty, the drops were formed on a restraining platform (ref. 14) rather than a flat surface. Enough material was used so that the drop that finally formed had an obtuse angle. (If a drop is formed carefully, it does not run over the sides due to the reluctance of the line of contact of a liquid and solid to cross a sharp edge (ref. 15).

The necessary dimensions of the drop were obtained by photographing the drops with a Praktina FX 35mm camera and enlarging the images on Kodak metallographic plates. A photograph of such a sessile drop is shown in figure 16. Figure 17 shows the necessary dimensions for calculating the surface tension by the Bashforth and Adams method. It is used in conjunction with the following equation:

$$\gamma = \frac{g\rho b^2}{\beta} \quad , \tag{18}$$

where g is the acceleration due to gravity; ρ, the density; b, the radius of curvature of the drop at the point where its surface cuts the axis of rotation; and β, the shape factor. The measured parameters are used to obtain b and β from the Bashforth and Adams tables.

Figure 18 shows the parameters used in the Dorsey method that utilizes the following equation:

$$\gamma = g\rho x^2 \left[\left(\frac{0.0520}{f}\right) - 0.1227 + 0.0481 f \right] \quad , \tag{19}$$

where x is the radius at the plane of the maximum diameter, $f = \frac{y}{x} - 0.4142$, and

y is the distance from the apex of the drop to the intersection of a 45-degree tangent with the principal axis.

WADD TR 60-463 Pt. II   -31-
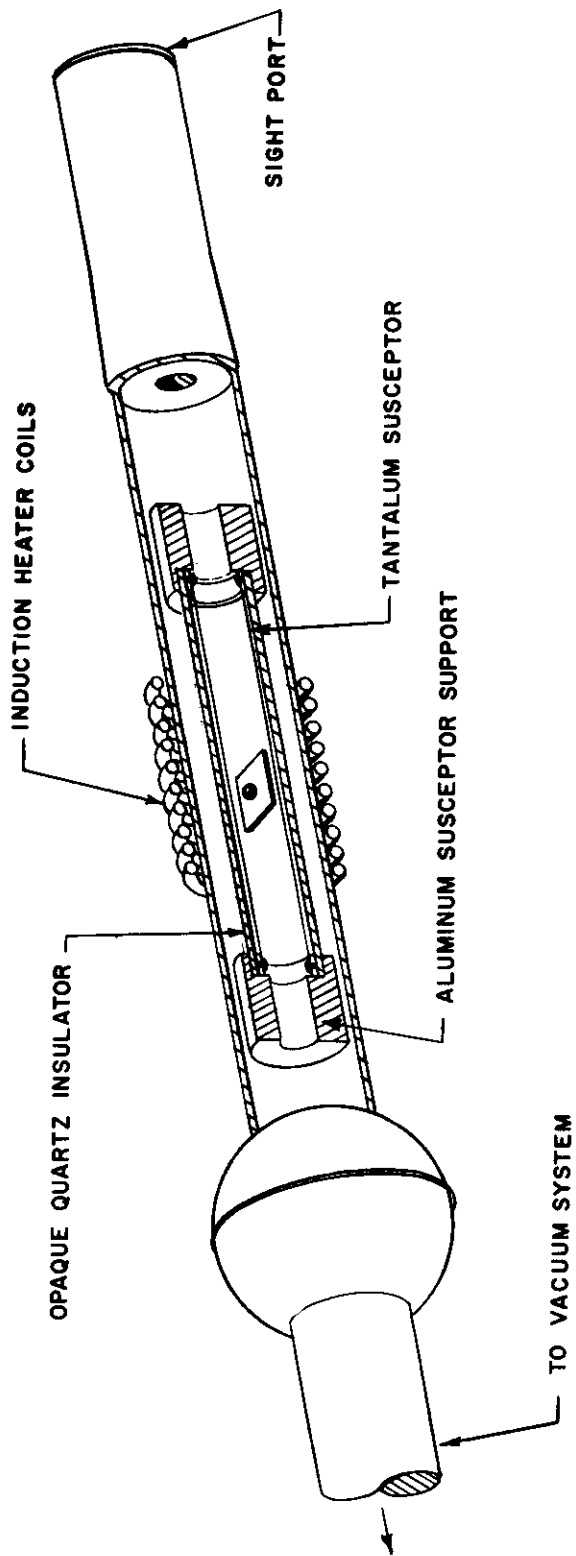
Figure 15 Sessile drop apparatus

SIGHT PORT

INDUCTION HEATER COILS

TANTALUM SUSCEPTOR

ALUMINUM SUSCEPTOR SUPPORT

OPAQUE QUARTZ INSULATOR

TO VACUUM SYSTEM

Figure 16   Photograph of a sessile drop

HEIGHT OF DROP ABOVE MAXIMUM DIAMETER

Z

RADIUS IN THE PLANE OF THE MAXIMUM DIAMETER

X
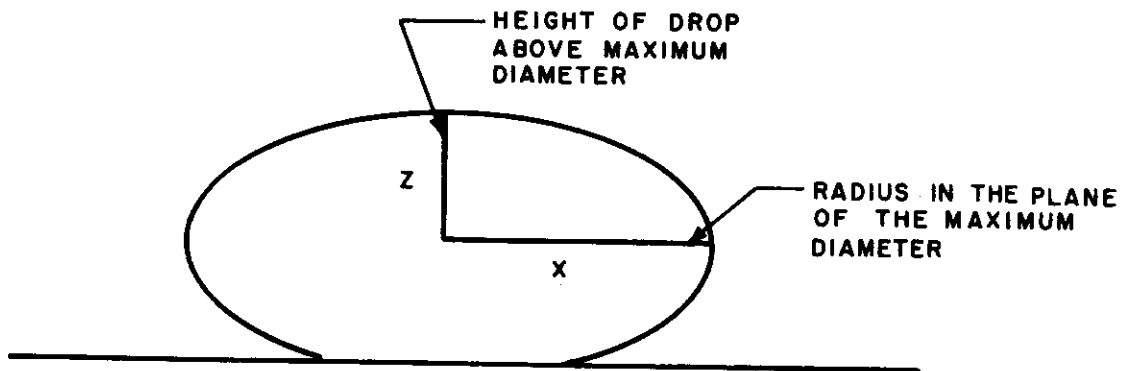
Figure 17 Sessile drop parameters used in the Bashforth and Adams method
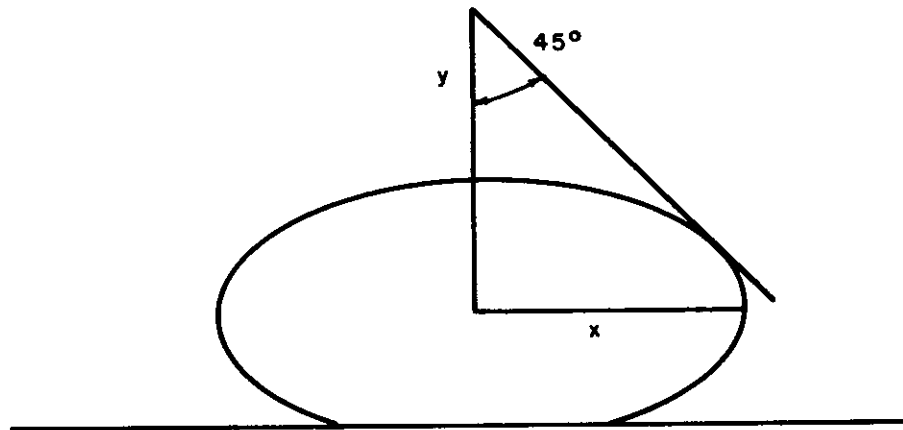
Figure 18 Sessile drop parameters used in the Dorsey method

The following is a typical calculation of SiO_2 plus 1 percent CoO, using both methods:

Bashforth & Adams,

$$Z = .3083 \text{ cm} \qquad \beta = 1.0 \qquad \rho = 1.984 \text{ gm/cm}^3$$

$$X = .3564 \text{ cm} \qquad b = .4021 \text{ cm} \quad b^2 = .1616 \text{ cm}^2$$

$$\gamma = \frac{980 \text{ cm/sec}^2 \times 1.984 \text{ gm/cm}^3 \times .1616 \text{ cm}^2}{1.0} = 314 \text{ ergs/cm}^2 \quad , \tag{20}$$

and

Dorsey,

$$\frac{y}{x} = .4519 \qquad f = .0377 \qquad x^2 = .1270 \text{ cm}^2$$

$$\gamma = 980 \text{ cm/sec}^2 \times 1.984 \text{ gm/cm}^3 \times .1270 \text{ cm}^2 \times 1.259$$

$$\gamma = 310 \text{ ergs/cm}^2 \tag{21}$$

Table 4 lists the surface tensions that have been obtained under this program by the Bashford and Adams method.

TABLE 4   SURFACE TENSIONS OF VARIOUS REFRACTORIES

Substance		Substrate	Surface Tension ergs/cm^2
Temperature higher than melting point	Silicia + 1% V_2O_5	W	498
	Silicia + 1% C_oO	W	314
	Silicia + 1% Cr_2O_3	W	424, 500
	Silicia + 1% Al_2O_3	W	473, 580
	Silicia + 1% M_gO	W	590
	Silicia + 1% ZrO_2	W	800
	Pure SiO_2 1830°C	W	370
	Pure SiO_2 1850°C	W	351
	Pure SiO_2 1865°C	W	281
	Pure SiO_2 2140°C	W	320
	Pure SiO_2 2250°C	W	278
	Zr + 10% U 1800°C	ThO_2	1300, 1370

WADD TR 60-463 Pt. II

III. VISCOSITY STUDIES

The counterbalanced sphere and oscillating bob techniques (ref. 1) were used to determine the viscosities of silica plus 1 percent Al_2O_3 , silica plus 1 percent V_2O_5 pure silica, and pure alumina. The results for the silica based refractories are shown in figure 19 and were determined by the counterbalanced sphere technique.

The viscosity of alumina at a temperature of approximately 2400^oK was determined to be between 1 and 10 poises. A 25 percent volume expansion on heating (ref. 16) and bubble formation in the melt make it difficult to improve the precision of this determination.

An attempt to measure the viscosity of zirconium with 10 percent uranium* by the oscillating bob technique, using thoria crucibles and thoria rods, yielded a maximum value of 1.5 poises at approximately 2300^oK. There was an interaction between the thoria rod and the melt, causing the rod diameter to decrease by about a factor of two and the apparent viscosity to decrease by this same ratio. Therefore, the value of 1.5 poises is being offered, with reservations, as an upper limit to the viscosity of this melt.

WADD TR 60-463 Pt. II

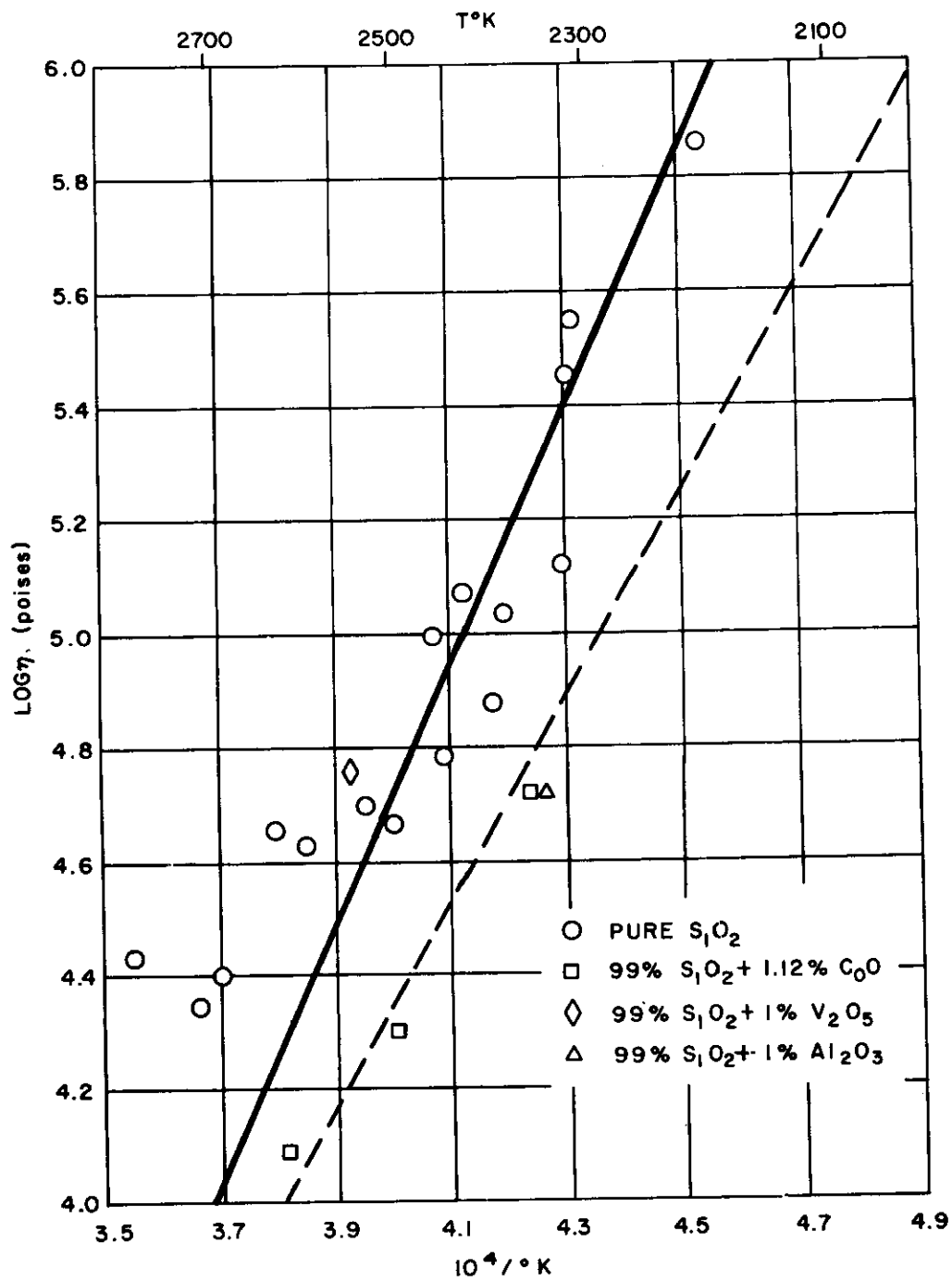Figure 19 Viscosities of materials tested

APPENDICES

A. A HIGH TEMPERATURE KNUDSEN EFFUSION SAMPLING SYSTEM

B. VAPORIZATION OF IRIDIUM AND RHODIUM

C. THE VAPORIZATION OF ALUMINA (Al_2O_3)

D. THE VAPORIZATION OF SEVERAL RARE EARTH OXIDES

E. THE VAPORIZATION OF THE RARE EARTH OXIDES

F. CONTINUOUSLY MONITORED EVAPORATION

APPENDIX A. A HIGH TEMPERATURE KNUDSEN EFFUSION SAMPLING SYSTEM

by M. B. Panish and L. Reif

A. ABSTRACT

A simple electron-beam furnace for Knudsen effusion studies is described. Temperatures as high as 2700 °K have been maintained in this system at pressures of the order of 10^{-6} mm Hg.

B. INTRODUCTION

Few methods lend themselves to the successful measurement of the vapor pressure of materials that vaporize appreciably only at very high temperatures. At very low pressures and high temperatures, the most used and most practical methods are based upon Langmuir rate of vaporization techniques (ref. 17) or Knudsen effusion techniques (ref. 18). Unlike the nonequilibrium Langmuir method, the Knudsen effusion method frequently permits a close approach to equilibrium in the vaporizing system. The effusion technique has been used to great advantage in numerous vapor pressure studies (refs. 19, 20).

The use of the time-of-flight mass spectrometer for the study of the vaporization of materials at very high temperatures has led to the development of a very simple electron bombardment furnace. Although such furnaces are not new, a detailed description of a very simple laboratory device is not available.

C. DESCRIPTION OF THE FURNACE

The electron bombardment furnace described here is used in conjunction with a modified Bendix time-of-flight mass spectrometer. As shown in figure 20, it consists essentially of a water-cooled baffle, an electrical shield, two 10-mil tungsten filaments, and the Knudsen effusion cell. The effusion cell is supported by a thin tungsten rod to ensure a minimum loss of heat by thermal conduction.

Heating of the electrically grounded effusion cell is achieved by bombarding it with electrons emitted from the negatively charged tungsten filaments. The filaments are heated to emitting temperatures by a simple filament supply (providing 5 to 10-amp a c to each filament) that can be isolated from ground. One side of each of the filaments is attached to the electrostatic shield.* The negative high voltage is supplied through the shield which thus prevents the emitted electrons from migrating to other parts of the system.

A typical curve of the power input (high voltage times emission current) versus temperature of a small effusion cell is given in figure 21. For the various

---

*The filaments were attached to the electrostatic shield and to the nickel or steel support rods by spot welding under a stream of argon. The electrostatic shield is a cylinder of molybdenum rolled from 20-mil molybdenum sheet and spot welded (under argon) to the steel supporting members that are insulated from the rest of the system.

LIQUID NITROGEN

VAC-ION
PUMP

STEEL VACUUM
SYSTEM

MASS
SPECTROMETER
ION SOURCE

ENTRANCE
SLIT

SHUTTER

OBSERVATION
PORT

BLACK BODY HOLE

EFFUSION CELL

FILAMENT

WATER COOLED
BAFFLE (GROUNDED)

MOLYBDENUM ELECTROSTATIC
SHIELD - SUPPORTED ON
INSULATED POST

SUPPORT
ROD
ANCHORED
TO
GROUND

TO-H.V.

VAC-ION
PUMP

LIQUID NITROGEN

INSULATED
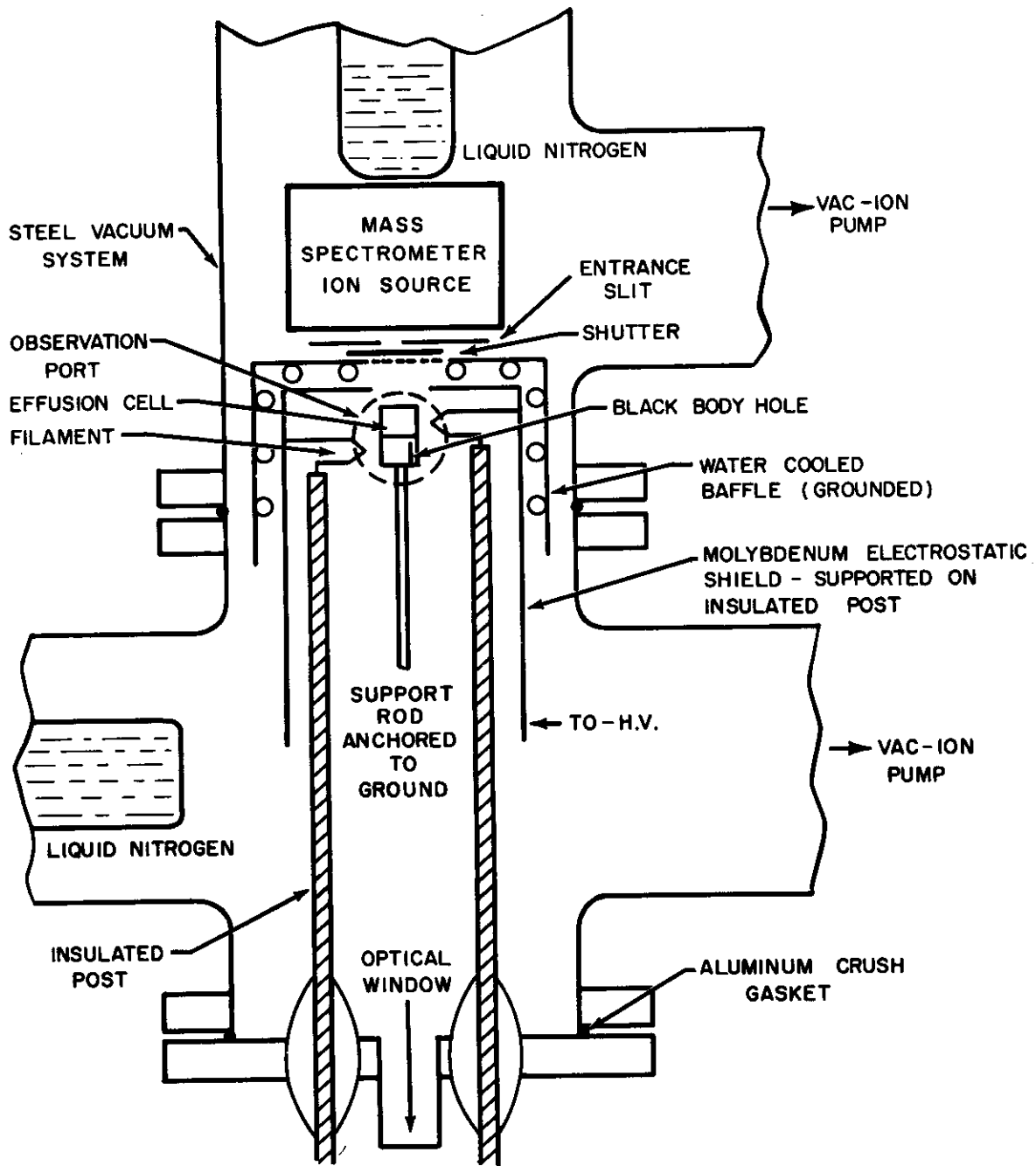POST

OPTICAL
WINDOW

ALUMINUM CRUSH
GASKET

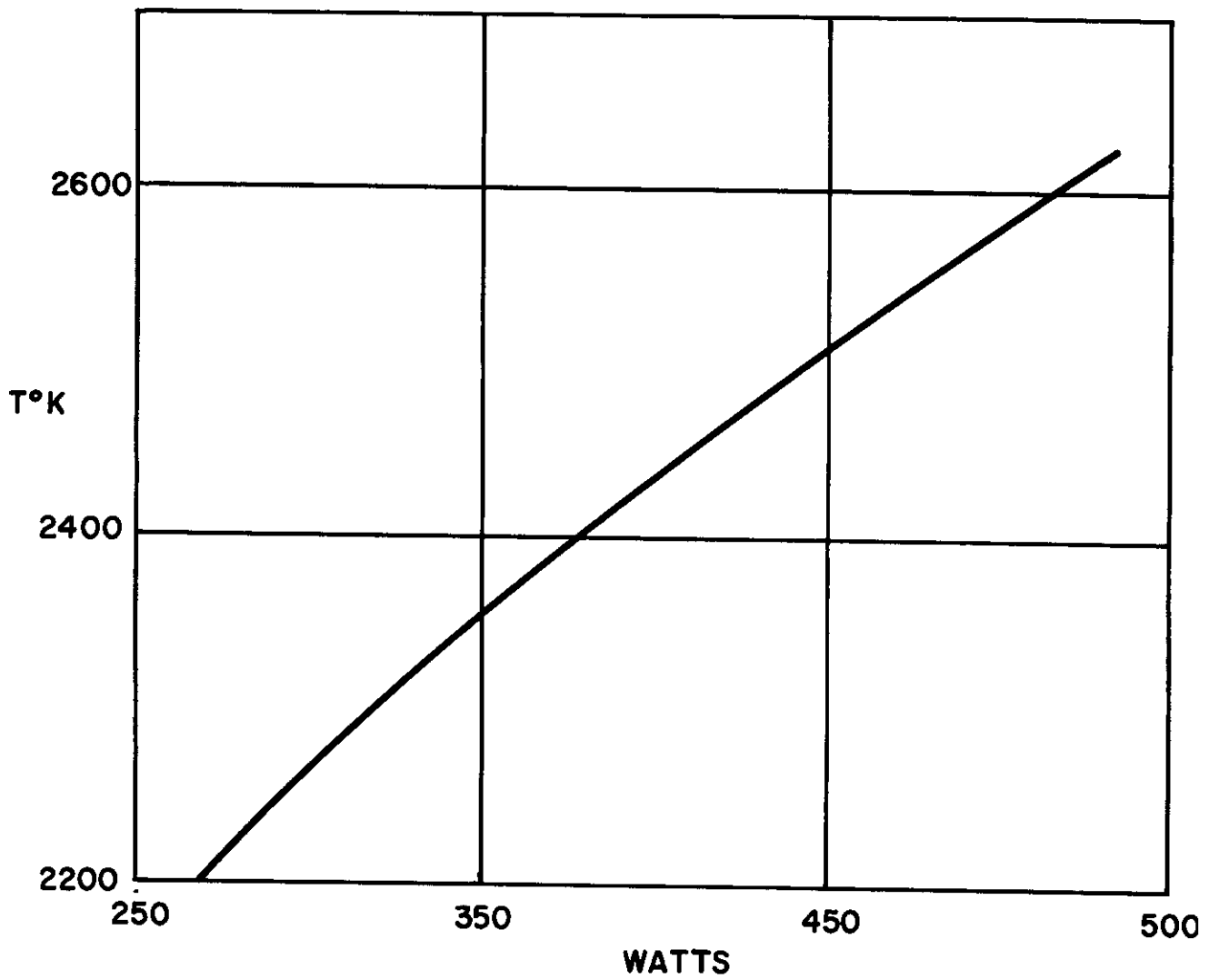Figure 20 Electron-beam furnace attached to time of flight spectrometer

Figure 21 Power input into an effusion cell of 5.5cm^2 surface area

effusion cells used in this system, voltages up to 2000 volts and emission currents up to 1 ampere have been used.

D. THE EFFUSION CELL

As may be seen in figure 22, the effusion cell is divided into two parts, each of which is heated primarily by electron-bombardment from one of the filaments. The cell halves are held at the same temperature by manual regulation of the heater current to each of the two filaments. This has been checked by determination of the surface brightness of both parts of the crucible through an observation port. The total power is varied by adjusting the negative voltage on the heater and shield.

Due to the lack of radiation shielding in this effusion cell, it is necessary to use a higher energy input than in more heavily shielded systems. Thick cell walls are the major means of providing an even temperature distribution, although the overlap in the electron bombardment from the filaments is also helpful. In general, with cell wall thicknesses of approximately 3/32 in. and cell diameters not greater than 1/2 in., it has been possible to maintain temperatures as high as 2700°K, with a temperature variation across the cell of approximately 10°K. The temperature of the effusion cell is measured with a micro-optical pyrometer, using the radiation emitted by the small blackbody hole shown in figure 22. Figure 22 also shows typical cell liners. Thoria liners have been found useful for the study of the vaporization of many metals.

E. EVACUATION AND HEATING

It is generally useful in mass spectrometric studies to employ separate pumping systems for the spectrometer and the electron-bombardment furnace, as shown in figure 20. Two 75 liter/sec Vac-Ion pumps are mounted on the system used in our laboratories. When the effusion cell is cold and the system is clean, it is possible to achieve pressures of the order of 10^{-8} mm Hg or less.

The liquid nitrogen cold fingers shown in figure 20 are used to speed up the evacuation with the roughing pumps. It is generally possible to degas the cell at roughing pump pressures of approximately $\frac{1}{2}\mu$ at temperatures as high as 1800°K by heating with electron bombardment. The ultimate temperature that may be reached depends upon the material of which the effusion cell is constructed and the materials under study. It is possible to reach temperatures as high as 2700°K at pressures of the order of 10^{-6} mm Hg or lower with the system shown in figure 20 when the effusion cell is constructed of tungsten and the electrostatic shield of molybdenum.

It is possible for some purposes, to use a simpler electron bombardment system in which one side of each filament is grounded, and the crucible is insulated from ground and maintained at a high positive voltage. In this case, the electrical shield shown in figure 20 is not necessary. This system does not appear

THO$_2$ INNER LINER

$\frac{1"}{16}$

$\frac{3"}{16}$

$\frac{3"}{16}$

TUNGSTEN
CONTAINER

BLACK BODY HOLE

EFFUSION CELL SUPPORT ROD

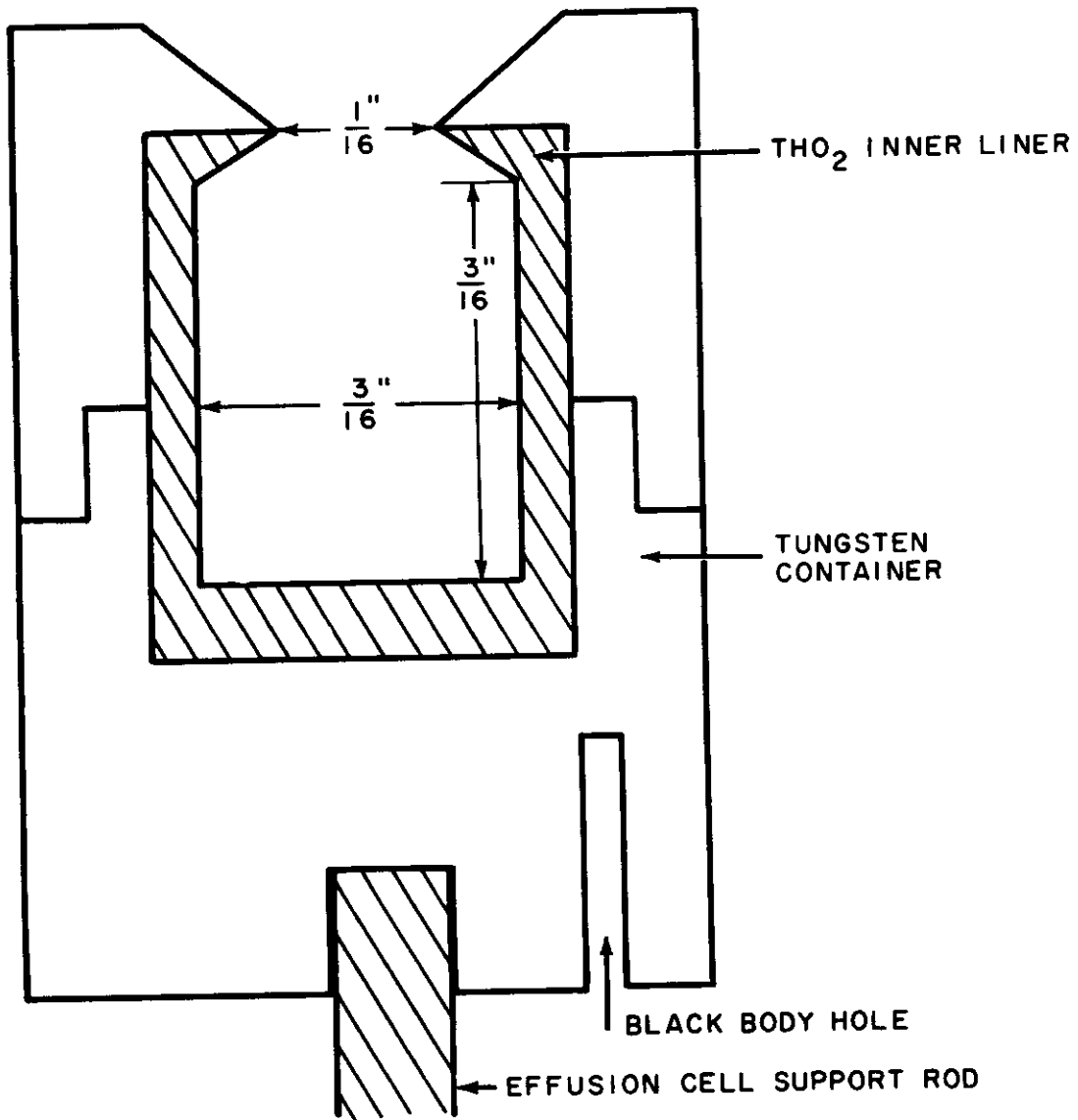Figure 22 Effusion cell

to be practical for mass spectrometric studies, however, as in some materials, surface ionization occurs and the resultant positive ions cause electrical disturbances in the mass spectrometer. Such a system has, however, been used in this laboratory for effusion studies in which the effusion beam was condensed on a liquid-nitrogen-cooled target (ref. 21).

F. ACKNOWLEDGMENTS

APPENDIX B. VAPORIZATION OF IRIDIUM AND RHODIUM

by M. B. Panish and L. Reif

A. ABSTRACT

The vaporization of iridium and rhodium have been studied by Knudsen effusion and Langmuir evaporation techniques. The vapor pressure of iridium over the temperature range of from 2100° to 2600°K is represented by the equation: $\log P_{mm} = 10.46 - (33,980/T)$, and the vapor pressure of rhodium over the temperature range of from 2050° to 2200°K by the equation: $\log P_{mm} = 10.28 - (28,300/T)$. Third law analyses of the data yield the following heats of vaporization: iridium, $\Delta H_{298} = 158.4 \pm 0.5$ kcal/mole; rhodium, $\Delta H_{298} = 132.8 \pm 9.3$ kcal/mole. Estimated boiling points for iridium and rhodium are 4800° and 3980°K, respectively.

B. INTRODUCTION

Although a great deal of information has been obtained on the vaporization of many of the more refractory metals, surprisingly little work has been done on the higher melting platinum metals.

There are only a limited number of vapor pressure measurement methods that are applicable, with a reasonable assurance of success, to materials that do not vaporize appreciably, except at very high temperatures. At very low pressures and high temperatures, the methods most used and most practical are based upon Langmuir's rate-of-evaporation measurements (ref. 17) or Knudsen effusion techniques (ref. 18).

In Langmuir rate-of-evaporation studies, the material to be studied is heated in a vacuum in such a manner that virtually all the material that leaves the heated surface condenses elsewhere in the system. The vapor pressure of the material is then obtained by determination of the loss of mass of the heated sample by use of the equation,

$$n = paA (2\pi MRT)^{-\frac{1}{2}} ,$$

(22)

where n is the number of moles per second which leave the surface of area A (cm^2) , M is the molecular weight of the gaseous species, R the gas constant, T the temperature in °K, a the accommodation coefficient, and p the equilibrium vapor pressure.

In this work it is assumed that $a = 1$; that is, that in a vacuum and at equilibrium vapor pressure the rate at which molecules leave the surface is the same.

The Knudsen effusion technique requires that the material to be studied be placed in an effusion cell. The effusion cell is, in the ideal case, an inert container

with a small orifice. If certain geometrical considerations are met, the number of moles per second of material that effuse from the cell and pass through a collimator whose axis is normal to and concentric with the center of the orifice is:

$$n = paD^2 (2\pi MRT)^{-\frac{1}{2}}/(D^2 + 4L^2). \tag{23}$$

Where then, p is the pressure (d/cm^2), a the orifice area (cm^2), D the collimator diameter (cm), L the collimator to orifice distance (cm), M the molecular weight of the effusing species, R the gas constant, and T the temperature (^oK).

Detailed descriptions of both methods, discussions of the limiting assumptions, and derivation of the equations from the kinetic theory of gases are available in several standard reference works (refs. 19, 22).

C. EXPERIMENTAL

1. Knudsen Effusion Studies

A thoria lined tungsten effusion cell was used in the effusion experiments. The molecular beam effusing from the cell orifice passed through a collimator and struck a cooled target. The rate of effusion of material from the cell was found by determining the amount of material that had condensed upon the target, either by direct weighing of the target or by the use of a radioactive tracer.

The effusion cell used for the iridium is the same as that shown in figure 4 except that the iridium liner was removed. It was heated by electron bombardment from two filaments that heated the upper and lower halves independently of each other. Temperature was measured with a micro-optical pyrometer from light collected from the blackbody hole. The optical system and pyrometer were calibrated by measuring the brightness temperature of a tungsten ribbon lamp that had been calibrated by the National Bureau of Standards. The cell halves were held at the same temperature by manual regulation of the power to the two filaments, based upon temperature checks of the cell halves through an observation port in the vacuum system. Temperature in the blackbody hole was thus maintained at $T \pm 5^oC$, and the cell halves were held within 5° to 10^oC of each other during a run.

During a run, the effusion cell orifice was directly below the target magazine that contained a collimator and 12 copper target holders. These were in direct contact with the liquid-nitrogen-cooled copper walls of the magazine. The apparatus was constructed in such a manner that the target holders could be removed from the magazine after the targets had been

exposed to the effusion beam without breaking the vacuum. The targets themselves were discs of copper or platinum foil. A magnetically operated shutter could be moved between the effusion cell and the collimator to turn the beam on and off.

The quantity of iridium which had been deposited upon the targets was determined by the use of Ir^{192} as a radioactive tracer. The radioactivity of the target with the condensed sample was compared with that of a previously calibrated sample. This sample contained the same ratio of tracer to natural isotopes and a known total weight of the reference material. A standard-well-type crystal counter was used. No tracer was used for the studies of the vaporization of rhodium. In this case, the amount of rhodium deposited upon the target was determined directly by weighing the target before and after exposure to the beam. Weighing was done on a Sartorius microbalance to $\pm 5\mu g$. The targets were far enough away from the effusion cell so that Clausing corrections could be neglected.

The effusion cell used in the studies of the vapor pressure of rhodium was identical to that shown in figure 4, except that the thoria liner contained a cylindrical channel of 1/8 in. diameter and the iridium liner was omitted. The channel in this case was an excellent effusion cell since it was possible to pack the rhodium powder around its walls. The use of such an effusion cell was not possible with iridium powder because it tended to sinter into a small button when heated to very high temperatures in the 1/8 in. channel. This problem was not encountered when larger quantities of iridium powder were used in a cell with dimensions identical to those shown in figure 4.

2. Langmuir Vaporization Studies

To obtain a check upon the data obtained from the effusion studies, several data points were obtained for iridium by a Langmuir technique. An iridium cylinder, similar in construction to the lower half of the tungsten container shown in figure 22, was used. The cylinder was supported, heated, and its temperature determined in the same manner as for the effusion cells.

The total amount of material vaporized was determined by weighing the cylinder and the iridium support rod before and after each experiment. The vaporizing area was taken as the total outside area (including top and bottom) of a cylinder with the same radius and height as of the cell bottom used in the effusion experiment. The area of the support rod was neglected as there was a very large temperature gradient along its length, and its weight loss during a run was found to be negligible. If the accommodation coefficient of iridium for condensation upon itself at the temperature of the experiment is unity, the small additional area of the inside vertical walls of the depression in the top of the cylinder and the ridge on the top of the cylinder will make no additional contribution to the rate of vaporization.

Data from this study are more scattered than that obtained from effusion experiments because the cylinder could not be heated and cooled instantaneously, and because the temperature was determined with a precision of only $\pm$ 10°K. Iridium, vaporizing from the cylinder, condensed upon the cooled walls of the metal vacuum system, and any systematic error due to iridium bouncing back against the cylinder was negligible.

3. Mass Spectrometric Studies

To determine vapor pressure by both the Langmuir and Knudsen techniques, it is necessary to know what species are effusing from the cell or vaporizing from the surface. The vaporizing species could be observed by placing the effusion cell orifice or vaporizing surface close to the entrance slit of a Bendix time-of-flight mass spectrometer. Only monatomic species were observed for both iridium and rhodium.

D. RESULTS

1. Iridium

The vapor pressures calculated from equations (22) and (23) for the vaporization of iridium by Langmuir and Knudsen techniques are given in Table 5 and are plotted on figure 23 along with the estimated data of Stull and Sinke (ref. 2). The vapor pressures estimated by Stull and Sinke are apparently high because their calculations were based upon a low estimate of the boiling point of iridium. In the effusion studies, the points obtained when copper and platinum targets were used fall upon the same line. If any appreciable fraction of the molecules incident upon the target were reflected, it is probable that this would occur to a different degree for targets of different materials. On this basis, it has been assumed here that the amount of reflection was negligible.

The average heat of vaporization of iridium over the temperature range studied was found to be 155 $\pm$ 5 kcal/mole from the slope of a line drawn through the effusion data points. Stull and Sinke's $H_T^o - H_{298}^o$ data (ref. 2) were combined with this to yield a ΔH_{298} for sublimation of 158 $\pm$ 5 kcal/mole. The error was estimated by picking several possible lines through the points.

A more satisfactory method for checking the results of vapor pressure studies, such as that reported here is the so called third law calculation utilizing free energy functions (ref. 23).
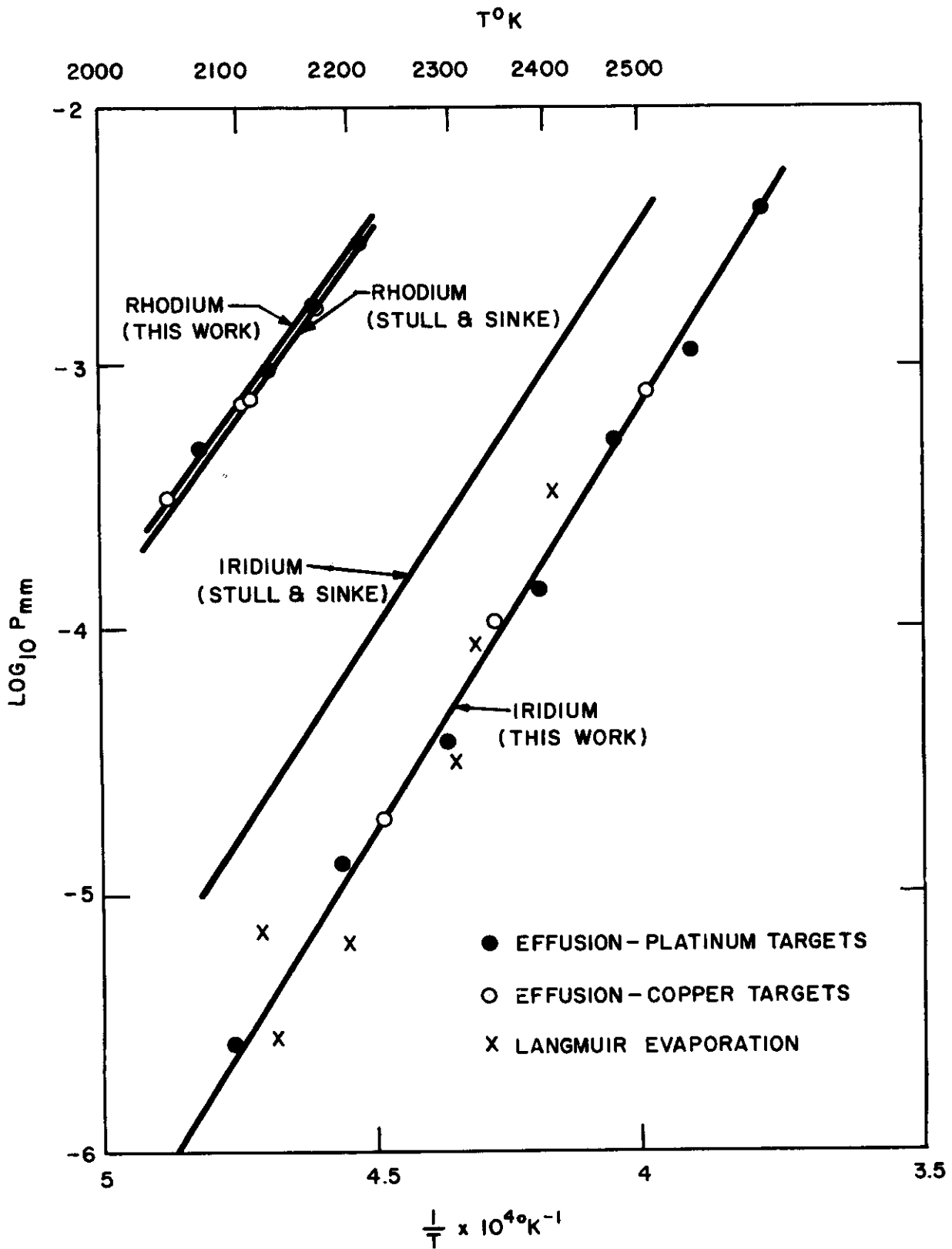
Figure 23 Log P versus 1/T for iridium and rhodium

For any reaction,

$$[(F_T - H_{298})/T]_{products} - [(F_T - H_{298})/T]_{reactants} = \left(\frac{\Delta F_T}{T}\right) - (\Delta H_{298}/T), \quad (24)$$

and

$$\left(\frac{\Delta F_T}{T}\right) = -R\ln K_{eq} \quad . \tag{25}$$

In this case $Ir_{(g)}$ is the product, $Ir_{(s)}$ is the reactant, and K_{eq} may be taken to be identical with P_{Ir}. The free energy functions for solid and gaseous iridium have been tabulated from heat capacity and spectroscopic data by Stull and Sinke. The results of third law calculations in which Stull and Sinke's free energy functions were used are also given in Table 5. Although the Langmuir data are quite scattered, they obviously agree quite well with the effusion data. Since this would be expected for a metal, the two methods serve as an excellent check upon each other. A further check is obtained by the excellent agreement between the slope and third law ΔH_{298} values. The measured pressures and calculated heats of vaporization obtained in this work are in essential agreement with those obtained with a Langmuir technique at lower temperatures by Hampson and (ref. 24).

The solid line drawn through the data points for iridium in figure 23 was obtained from equation (24), using $\Delta H_{298} = 158.4$ kcal/mole. This line is represented by,

$$\log_{10} P_{mm} = 10.46 - (33,980/T), \tag{26}$$

over the temperature range studied.

The boiling point of iridium was calculated by estimating the average heat of vaporization for liquid iridium from the melting point to $5000°K$. This quantity was used with vapor pressure at the melting point and the integrated Clausius-Clapeyron equation to obtain a boiling point of approximately $4800°K$.

2. Rhodium

The data obtained for the vaporization of rhodium by the effusion method are given in Table 6 and plotted on figure 23 along with the estimated vapor pressure data of Stull and Sinke. There is no appreciable difference between

the measured and estimated data. The third law calculations were done in a manner identical to those described for iridium. The average third law heat of vaporization of 132.8 ± 0.3 kcal/mole is in excellent agreement with that of 133 ± 2 kcal/mole obtained by the slope method.

The solid line drawn through the data point for rhodium in figure 23 was obtained from equation (24), using $\Delta H_{298} = 132.8$ kcal/mole . This line is represented by,

$$\log P_{mm} = 10.28 - (28,300/T), \tag{27}$$

over the temperature range studied. The boiling point of rhodium was estimated to be 3980°K, in a manner similar to that described for iridium.

E. ACKNOWLEDGMENTS

TABLE 5 IRIDIUM VAPORIZATION DATA

T °K	Experiment Type	P_{mm}	Target Material	ΔH_{298} 3rd law kcal/mole
2100	Effusion	2.29×10^{-6}	Pt	157.8
2196	Effusion	1.06×10^{-5}	Pt	158.2
2228	Effusion	1.69×10^{-5}	Cu	158.6
2282	Effusion	3.43×10^{-5}	Pt	158.9
2337	Effusion	9.40×10^{-5}	Cu	158.1
2375	Effusion	1.30×10^{-4}	Pt	159.0
2454	Effusion	4.76×10^{-4}	Pt	157.8
2492	Effusion	7.45×10^{-4}	Cu	158.0
2545	Effusion	1.04×10^{-3}	Pt	159.7
2630	Effusion	3.82×10^{-3}	Pt	158.1
	(Effusion) Av ΔH_{298} = 158.4 $\pm$ 0.5 (kcal/mole)			
2123	Langmuir	7.04×10^{-6}	...	155.0
2128	Langmuir	2.77×10^{-6}	...	159.2
2193	Langmuir	6.36×10^{-6}	...	161.3
2293	Langmuir	3.18×10^{-5}	...	160.0
2320	Langmuir	8.45×10^{-5}	...	157.4
2391	Langmuir	3.32×10^{-4}	...	155.6
	(Langmuir) Av ΔH_{298} = 158.1 $\pm$ 2 (kcal/mole)			

TABLE 6 RHODIUM VAPORIZATION DATA

T °K	P_{mm}	Target Material	ΔH_{298} 3rd law kcal/mole
2051	3.20×10^{-4}	Cu	132.4
2077	4.88×10^{-4}	Pt	132.4
2106	7.50×10^{-4}	Cu	132.6
2111	7.66×10^{-4}	Cu	132.8
2130	9.89×10^{-4}	Pt	132.9
2168	1.71×10^{-3}	Cu	133.0
2182	1.70×10^{-3}	Pt	133.8
2205	3.05×10^{-3}	Pt	132.8
Av ΔH_{298} = 132.8 $\pm$ 0.3 kcal/mole			

APPENDIX C. THE VAPORIZATION OF ALUMINA (Al_2O_3)*

by M. B. Panish and L. Reif

In a mass spectrometric study of the vaporization of Al_2O_3 from tungsten effusion cells, Drowart, DeMaria, Burns, and Inghram (ref. 25) concluded that alumina vaporized to yield principally Al and O, with much smaller amounts of Al_2O, AlO, and Al_2O_2. Similar studies with iridium effusion cells yield data that is essentially in agreement with that of Inghram.

In this work, the cell consisted essentially of an iridium cylinder containing a cavity 1/4 in. high and 1/4 in. in diameter with a 1/8-in. knife edged orifice. The cell was placed immediately below the entrance slit of a Bendix time-of-flight mass spectrometer from which it could be separated by a magnetically operated shutter.

Calibration of the mass spectrometric ion currents was obtained by performing an effusion experiment with Al_2O_3 in a tungsten cell of the same dimensions as the iridium cell. In the calibration run, a small portion of the effusing beam was condensed upon a liquid nitrogen cooled target, and the amount of material deposited was determined by weighing. Tungsten effusion cells were used for these calibrations because the iridium cells tended to fail structurally when maintained at very high temperatures for extended periods of time. Also, because a large quantity of iridium metal deposited upon the target. The methods of heating and temperature measurement have been described previously (ref. 21).

Since the principal mode of vaporization of Al_2O_3 has already been established as decomposition to Al and O, it has been assumed here that the Al pressure in the iridium cell is virtually the same as in the tungsten cell. The amount of Al that had deposited upon the targets was determined by subtracting that fraction which was due to Al_2O, AlO, and WO_2 from the total weight of material deposited. This was determined by independent mass spectrometric studies of the spectra from the tungsten cell and by the use of radioactive tungsten inside the cell in some of the calibration experiments. The amount of correction necessary was found to be approximately the same from both the mass spectrometric studies and the simple effusion experiments in which radioactive tungsten was used.

The ion currents (I^+) obtained from the iridium cell experiment were used with the atomic cross sections (σ) of Otvos and Stevenson (ref. 26) to obtain the pressures of AlO and Al_2O at a given temperature by the use of the relationships:

$$P_{AlO} = \frac{I^+_{AlO} \; \sigma_{Al}}{I^+_{Al} \; \sigma_{AlO}} \; P_{Al} , \tag{28}$$

and

$$P_{Al_2O} = \frac{I^+_{Al_2O} \; \sigma_{Al}}{I^+_{Al} \; \sigma_{Al_2O}} \; P_{Al} , \tag{29}$$

where P_{Al} then, is the pressure of aluminum obtained from the calibration experiments.

In figure 24, $\log p$ versus $1/T$ plots for the Al_2O_3 - W studies are plotted along with the data for AlO and Al_2O, obtained from the mass spectrometric studies with iridium effusion cells. If the species within the cell are in equilibrium, the pressure data may be used to determine some of the thermodynamic properties of AlO and Al_2O. Since the data for AlO and Al_2O are quite scattered, the slope method for the calculation of thermodynamic properties was not used. Instead, pressures and temperatures for third law calculations were selected from the approximate curves plotted in figure 24, and are presented, along with the estimated errors in Tables 7 and 8. The $\Delta[(F - H)/T]$ values are due to Inghram (ref. 25). O^+ currents were not determined in this work. The equilibrium constants were determined after assuming that $P_O = 3/2\,P_{Al}$,

By combining Stull and Sinke's (ref. 2) data for the elements with the dissociation energies in Tables 7 and 8, the ΔH_f^0 values of AlO and Al_2O are found to be 32 ± 5, and -15 ± 7 kcal/mole, respectively, and the enthalpy of dissociation of $Al_2O_{(g)}$ to yield $AlO_{(g)}$ and $Al_{(g)}$ is found to be 125 ± 12 kcal/mole .

In addition to the work described above, an experiment using a baffled effusion cell was done. All vaporizing species had to strike a hot tungsten surface. In this case, lower ion currents of AlO^+, Al_2O^+ and WO_2^+ were observed than with normal cells. This indicates that equilibrium may not be attained when the normal cells are used.
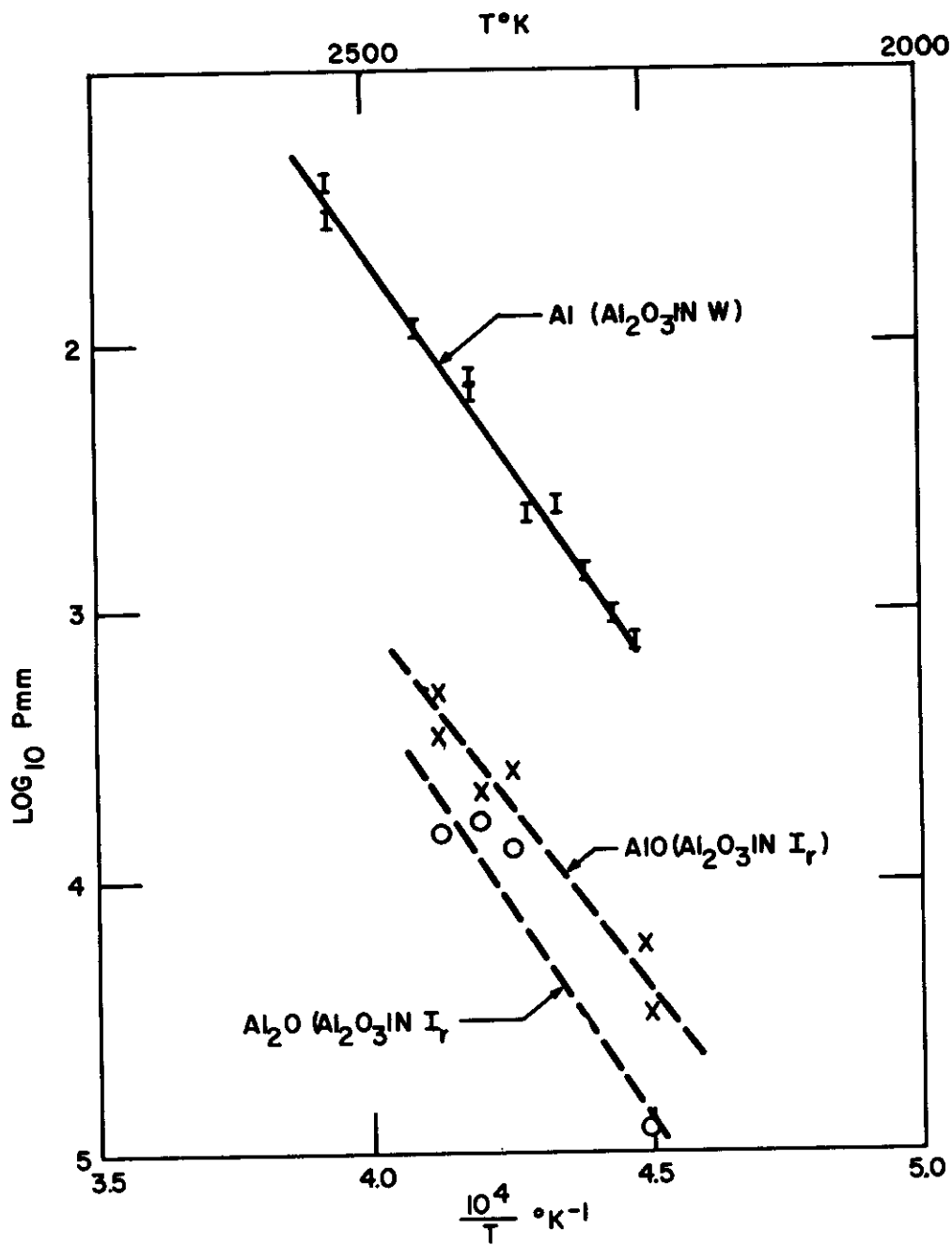
Figure 24 LogP versus 1/T plots for species vaporizing from Al_2O_3

TABLE 7 $Al_2O_{(g)} \longrightarrow 2Al_{(g)} + O_{(g)}$

T $°K$	$-\log P_{Al}$ mm	$-\log P_{Al_2O}$ mm	$-\Delta\left(\dfrac{F-H°}{T}\right)^*$ eu	$-R \ln K_{eq}$ eu	ΔH_O kcal/mole
2300	2.77 ± 0.1	4.38 ± 0.3	57.5	43.1	232 ± 7
2400	2.18 ± 0.1	3.80 ± 0.3	57.6	38.1	230 ± 7
2500	1.68 ± 0.1	3.30 ± 0.3	57.7	33.6	229 ± 7
					Avg. 230 ± 7

* Data obtained from ref. 25.

Table 8 $AlO_{(g)} \longrightarrow Al_{(g)} + O_{(g)}$

T $°K$	$-\log P_{Al}$ mm	$-\log P_{AlO}$ mm	$-\Delta\left(\dfrac{F-H°}{T}\right)^*$ eu	$-R \ln K_{eq}$ eu	ΔH_O kcal/mole
2300	2.77 ± 0.1	4.0 ± 0.2	27.3	19.4	107 ± 5
2400	2.18 ± 0.1	3.5 ± 0.2	27.4	16.5	105 ± 5
2500	1.68 ± 0.1	3.0 ± 0.2	27.5	14.0	104 ± 5
					Avg. 105 ± 5

* Data obtained from ref. 25.

APPENDIX D. THE VAPORIZATION OF SEVERAL RARE EARTH OXIDES*

by M. B. Panish

The vaporization of two of the lightest rare earth oxides, La_2O_3 and Nd_2O_3 has been shown by several workers (refs. 27,28) to proceed principally by means of the reaction,

$$M_2O_{3(s)} \longrightarrow 2MO_{(g)} + O_{(g)} \quad . \tag{30}$$

The work of Chupka, Inghram and Porter was a mass spectrometric study of the $La-La_2O_3$ system. That of Walsh, Goldstein and White was a simple effusion study of La_2O_3 and Nd_2O_3, vaporizing from tungsten effusion cells.

In this work, the vaporization of Pr_2O_3, Nd_2O_3, Sm_2O_3, and Eu_2O_3 has been studied at temperatures ranging from 1950° to $2350^\circ K$, by analyzing the species effusing from a Knudsen effusion cell with a Bendix time-of-flight mass spectrometer. Experimental details of the heating and temperature measuring techniques were described previously (ref. 21).

The effusion cells were lined with either iridium or thoria. Studies in which iridium liners were used were principally to determine the relative amounts of the various species in equilibrium with the oxide with a minimum of chemical interference from the container. The ratio I_{M^+}/I_{MO^+} of ion currents, due to the metal and monoxide when 20 ev electrons were used, are given in the last column in Table 9. A search for effusing species was made at several temperatures and electron-bombardment energies for each of the compounds studied.

If the ion current ratios in Table 9 represent the ratios of the equilibrium species in the effusion cell, it is obvious that among the oxides studied there is a change in the vaporization mode from that shown in equation (30) to that shown in equation (31), with increasing atomic number of the rare earth metal,

$$M_2O_{3(s)} \longrightarrow 2M_{(g)} + 3O_{(g)} \tag{31}$$

Spurious results would be expected if the observed ions did not originate from simple ionization of neutral species, but from dissociative ionization of a parent molecule or by ion molecule combination in the ion source. In all the cases presented here, ion molecule combination is highly improbable because of the low concentration of ions and molecules in the ion source. If the MO^+ ions were due to dissociative ionization, ions of higher mass would be present in appreciable amounts. This is not the case.

The M^+ ions observed when vaporizing Sm_2O_3 and Eu_2O_3 could have derived from dissociative ionization. To determine which process led to the formation of

these ions, Sm_2O_3 and Eu_2O_3 were vaporized from ThO_2 effusion cells containing a small amount of SiO_2. The vaporization thus occurred in an oxidizing atmosphere. Under these conditions, the MO^+ ions, rather than M^+ ions, were the major species observed. It follows that the M^+ ions observed as the major, or as an important species under neutral conditions, were due principally to simple ionization of the parent M atoms in the effusion beam.

The vaporization of the oxides under neutral conditions appeared to be stoichiometric. X-ray analyses of the oxides after heating indicated that only M_2O_3 was present at the end of the run.

To determine the approximate equilibrium pressures of the vaporizing species, mixtures of the oxide and rhodium powder were effused from thoria-lined cells. The rhodium provided an internal calibration by which the pressure of the species could be calculated from:

$$P_X = \frac{I_X^+ \, \sigma_{Rh}}{I_{Rh}^+ \, \sigma_X} \, P_{Rh} \, , \tag{32}$$

where P, σ, and I^+ are the vapor pressures, electron cross sections, and ion currents of the species X and rhodium. Iridium, vaporizing from the liner in the first experiments, could not be used for calibration because of its low vapor pressure (ref. 21). The vapor pressures of rhodium estimated by Stull and Sinke (ref. 2), and confirmed in this laboratory (ref. 21), were used.

The electron cross sections of rhodium, the rare earth metals, and oxygen were taken as 40.6, 73, and 3.3, respectively, on the basis of the work of Otvos and Stevenson (ref. 26). It was assumed that the electron cross sections of the oxides were equal to the sums of the cross sections for the metals and oxygen. The uncertainties, included in the extrapolation of the data of Otvos and Stevenson, and in the assumption that electron cross sections are additive could, of course, have led to errors as large as a factor of 2 or 3 in the absolute pressure data. The values reported in Table 9 can, therefore, only be considered to be approximate ones.

It is assumed that the pre-degassed thoria liners did not interfere with these measurements. No condensed phase interaction was noted, and the equilibrium vapor pressure of $ThO_{(g)}$ and $ThO_{2(g)}$ with $ThO_{2(s)}$ was several orders of magnitude lower than that of the gaseous species of the least volatile of the compounds studied.* The ratios of the various species effusing from the thoria-lined cells were not markedly different from those obtained with the iridium cells.

---

*Panish, M.B. and L. Reif (see section I-D).

TABLE 9. EQUILIBRIUM VAPORIZATION DATA AT 2000°K

Oxide	P_M atm	P_{MO} atm	P_{MO_2} atm	I_M^+/I_{MO}^+
Pr_2O_3	$< 1 \times 10^{-8}$	1×10^{-7}	$< 5 \times 10^{-9}$	< 0.1
Nd_2O_3	$< 5 \times 10^{-9}$	5×10^{-8}	n. d.	< 0.1
Sm_2O_3	$\approx 3 \times 10^{-9}$	$\approx 3 \times 10^{-9}$	n. d.	$0.5 - 1.0$
Eu_2O_3	7×10^{-8}	9×10^{-9}	n. d.	8.0 ± 2

APPENDIX E. THE VAPORIZATION OF THE RARE EARTH OXIDES[*]

by M. B. Panish

The vaporization modes of most of the sequioxides of the lighter rare earth metals have previously been shown to change from

$$M_2O_3 \longrightarrow 2MO_{(g)} + O_{(g)} \qquad (33)$$

to

$$M_2O_3 \longrightarrow 2M_{(g)} + 3O_{(g)} \ , \qquad (34)$$

with increasing atomic number of the metal (ref. 29).

In this work we have studied the vaporization of Gd_2O_3, Tb_2O_3, Dy_2O_3, Ho_2O_3, Er_2O_3, Tm_2O_3, Yb_2O_3, and Lu_2O_3 at temperatures ranging from 2000° to 2500 °K by analyzing the species effusing from an iridium effusion cell with a Bendix time-of-flight mass spectrometer. Experimental details of the heating and temperature measuring techniques have been described previously (ref. 21).

The ratios of the ion currents due to the metal and the monoxide, I_{M^+}/I_{MO^+}, are shown in figure 25 for ions produced with a 20 electron volt electron beam. The previously reported data on La_2O_3, Pr_2O_3, Nd_2O_3, Sm_2O_3, and Eu_2O_3 (refs. 21, 28, 29) are also included in the figure. The effusing species were observed at several temperatures and electron-beam energies for each of the compounds studied. The variation of the ion current ratio with temperature over several hundred degrees also was found to be within the limits shown about each point in figure 25. The limits shown for the vaporization of Eu_2O_3 and Tm_2O_3 are quite large because the low concentration of MO obtained with these oxides necessitated measurements at low signal/noise levels. In the case of Yb_2O_3, only Yb^+ ions were observed.

The possibility that the results might have been seriously influenced by dissociative ionizations or ion molecule recombinations within the ion source was examined in a manner identical to that described previously (ref. 29). These processes were found to be insignificant. It thus appears that the rare earth sesquioxides may be divided into two groups, within each of which the vaporization mode changes from that shown in equation (33) to that shown in equation (34) with increasing atomic number of the rare earth metal. It is of interest to note the abrupt change in the vaporization mode that occurs after Eu and Yb, the rare earth metals, in which the 4f electron shell is half and completely filled. It is also of interest to note that except for Lu_2O_3, the classification of the oxides
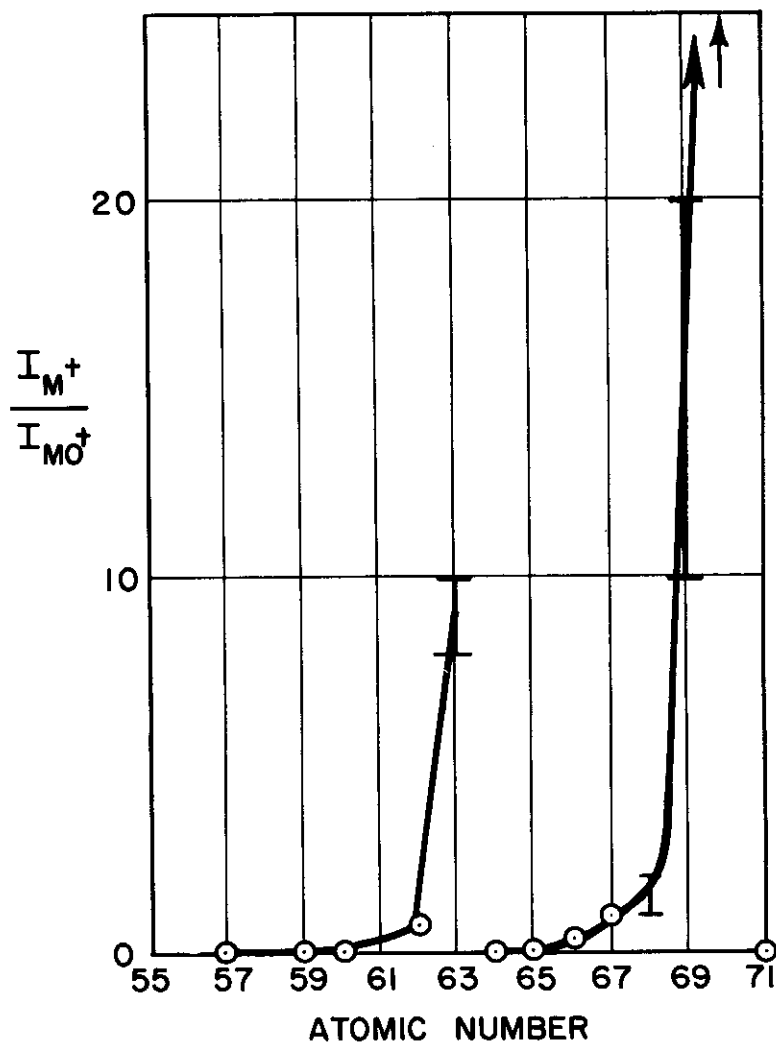
Figure 25 Ion current ratio $I_M{}^+/I_{MO}{}^+$ versus atomic number of M for the vaporization of M_2O_3

into groups according to their vaporization modes is identical to the separation of the rare earths into so-called cerium and yttrium groups according to their behavior in various separation schemes (ref. 30).

The approximate vapor pressures of the major species vaporizing from the yttrium group of oxides were determined in a manner similar to that described previously for the cerium group. The equilibrium partial pressures over M_2O_3 at 2300°K were: TbO, DyO, HoO, ErO, LuO $\approx 10^{-7}$ atm; Tm and Yb $\approx 10^{-6}$ atm. To obtain the approximate pressures, the iridium ion current from the vaporization of the iridium effusion cell was used for the calibration of the M^+ and MO^+ ion currents.

APPENDIX F. CONTINUOUSLY MONITORED EVAPORATION

The measurement of rates of effusion by the Knudsen technique is probably the most applicable method of obtaining the partial molar free energies of evaporation or decomposition of relatively stable refractories (ref. 31). These free energies, combined with aerodynamic considerations, are necessary for the calculation of equilibrium concentrations and reaction rates (ref. 32) in the rocket nozzle. In the conventional method of conducting an effusion experiment, the material to be tested is placed inside of an inert crucible containing an orifice of known dimensions, and the rate at which the material leaves the crucible is measured.

The Langmuir evaporation (ref. 31) technique has been used for those materials for which an inert crucible cannot be found or whose vapor pressure is too low. One of the difficulties with the use of the Langmuir method is that appreciable reductions in the rates of evaporation may occur for materials that evaporate by preferential volatilization of some of their components (ref. 33). These changes in rates of evaporation are due to changes in the surface composition. In the usual method of conducting a Langmuir experiment, these changes in pressure due to changes in surface composition are not determined. Only the integrated weight loss over the time of the experiment is measured. Monitoring of the time dependence of the evaporation (refs. 34, 35, 36) has been proposed as a method of taking into account these changes in surface composition. By extending the argument of possibly accounting for changes in the surface composition by a measurement of the time dependence of the evaporation, continuous monitoring techniques are proposed as a rapid method of obtaining thermodynamic data of all of the various regions of a phase diagram.

In those cases where diffusional processes are rapid enough to compensate for evaporational processes, continuous monitoring can be used to obtain unknown phase diagrams as well as energies of formation. The vapor pressure, at any time, may be obtained from the volatility data and a knowledge of the vapor composition. The phase diagram may be obtained by an examination of the relation of the pressure to the composition of the condensed phase. The equilibrium form of a pressure-composition curve of a binary system is well known. It consists of a series of constant pressure plateaus in the heterogeneous phase fields connected by a series of descending curves in the homogeneous phase fields. The condensed phase composition may be calculated from the knowledge of the vapor composition, the condensed phase starting composition, and the weight loss data with the assumption that the surface composition is the same as that of the cell.
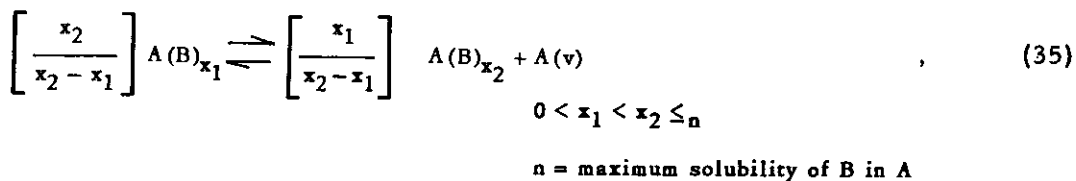
In those cases where diffusion is the rate-limiting step, information other than the time dependence of the evaporation and the starting compositions may be required to obtain the phase diagram and free energies of formation. The

assumption then, can no longer be made that the surface and interior compositions are the same. Information such as diffusion constants, X-ray diffraction, compositional analysis as a function of position in the sample, etc, will be needed.
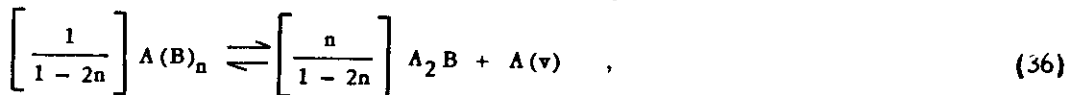
The arguments that follow are directly applicable only to the case of volume diffusion. The effects of grain boundary diffusion, transfer of material through pores or empty space between particles, will be ignored. In other words, the case will be considered where the vapor and condensed regions are separated by a surface, and where diffusion takes place only in the direction perpendicular to this surface. Also, the concentration is initially uniform in each region.

The system A-B, forming two compounds, A_2B and AB_2 should be considered. In the temperature region under discussion, only A is volatile. Assume that for the phase diagram shown in figure 26 only the following vaporization reactions may occur in the various phase fields:
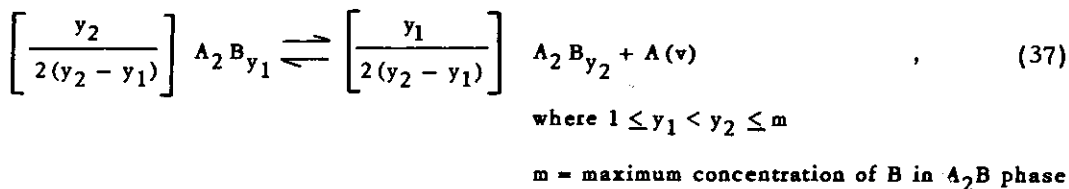
Homogeneous Phase Field A

$$\left[\frac{x_2}{x_2 - x_1}\right] A(B)_{x_1} \rightleftharpoons \left[\frac{x_1}{x_2 - x_1}\right] A(B)_{x_2} + A(v) \qquad , \qquad (35)$$

$$0 < x_1 < x_2 \leq n$$

n = maximum solubility of B in A

Heterogeneous Phase Field $A(B)_n$ and A_2B

$$\left[\frac{1}{1 - 2n}\right] A(B)_n \rightleftharpoons \left[\frac{n}{1 - 2n}\right] A_2B + A(v) \qquad , \qquad (36)$$

Homogeneous Phase Field A_2B

$$\left[\frac{y_2}{2(y_2 - y_1)}\right] A_2B_{y_1} \rightleftharpoons \left[\frac{y_1}{2(y_2 - y_1)}\right] A_2B_{y_2} + A(v) \qquad , \qquad (37)$$

where $1 \leq y_1 < y_2 \leq m$

m = maximum concentration of B in A_2B phase
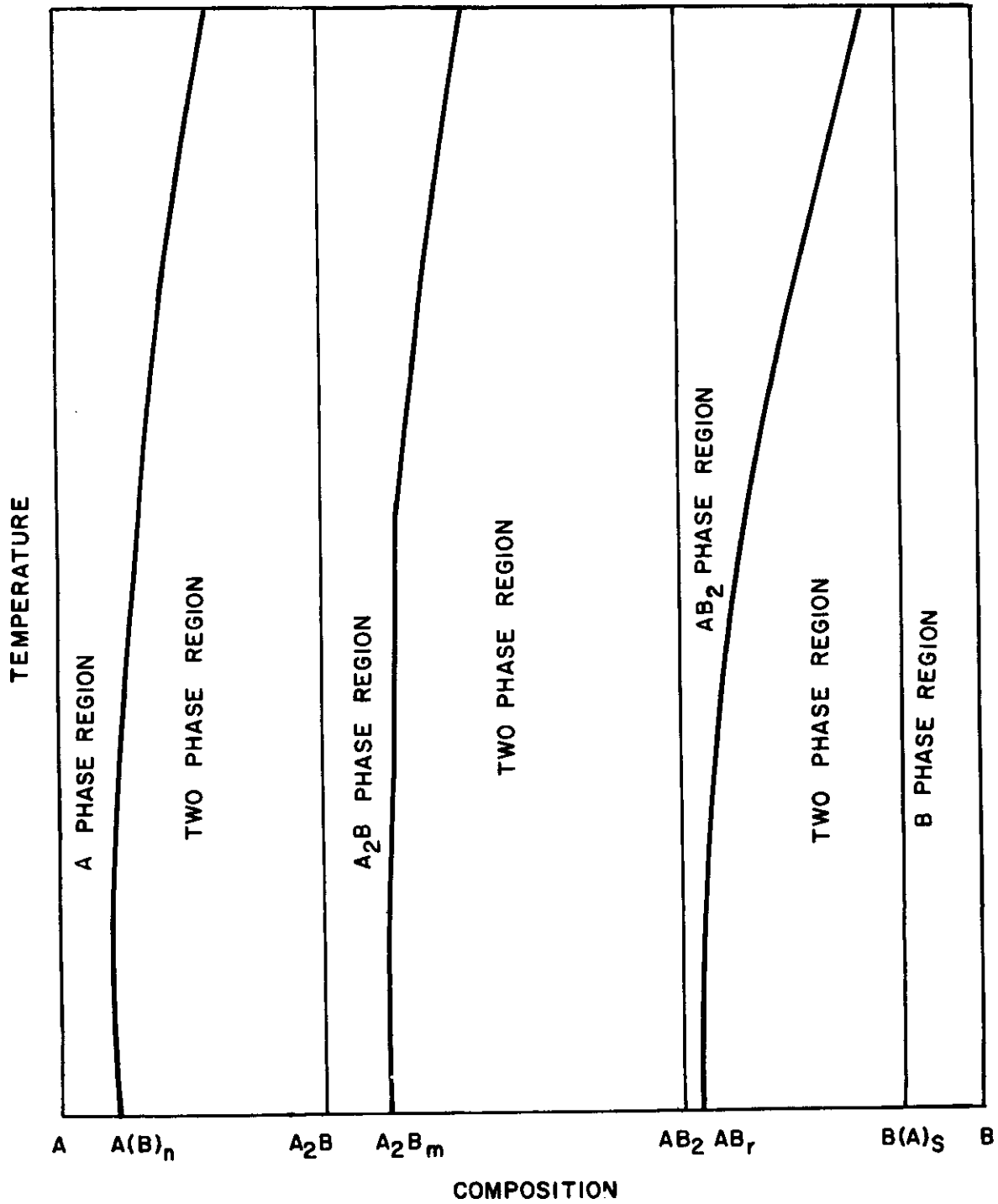
Figure 26 Phase diagram of system A-B

TEMPERATURE

A PHASE REGION

TWO PHASE REGION

A_2B PHASE REGION

TWO PHASE REGION

AB_2 PHASE REGION

TWO PHASE REGION

B PHASE REGION

A $\quad$ A(B)$_n$ $\quad\quad$ A_2B $\quad$ A_2B_m $\quad\quad$ AB_2 AB_r $\quad\quad$ B(A)$_S$ $\quad$ B

COMPOSITION

Heterogeneous Phase Field A_2B_m and AB_2

$$\left[\frac{2}{4-m}\right] A_2B_m \ \underset{\longleftarrow}{\overset{\longrightarrow}{}}\ \left[\frac{m}{4-m}\right] AB_2 + A(v) \ , \tag{38}$$

Homogeneous phase field AB_2

$$\left[\frac{q_2}{q_2-q_1}\right] AB_{q_1} \ \underset{\longleftarrow}{\overset{\longrightarrow}{}}\ \left[\frac{q_1}{q_2-q_1}\right] AB_{q_2} + A(v) \qquad , \tag{39}$$
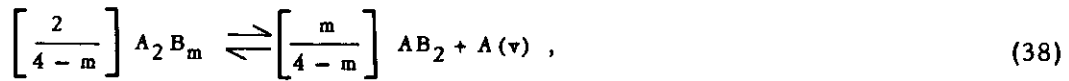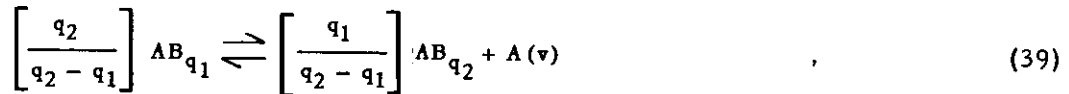
where $0 \leq q_1 < q_2 \leq r$

r = maximum concentration of B in AB_2 phase

Heterogeneous phase field AB_r and $B(A)_s$

$$\left[\frac{1}{1-rs}\right] AB_r \ \underset{\longleftarrow}{\overset{\longrightarrow}{}}\ \left[\frac{r}{1-rs}\right] B(A)_s + A(v) \qquad , \ \text{and} \tag{40}$$
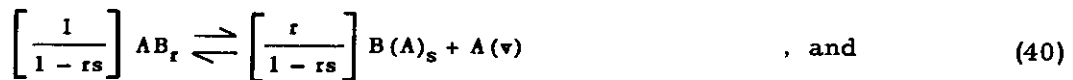
s = maximum solubility of A in B

Homogeneous phase field B

$$\left[\frac{1}{z_1-z_2}\right] B(A)_{z_1} \ \underset{\longleftarrow}{\overset{\longrightarrow}{}}\ \left[\frac{1}{z_1-z_2}\right] B(A)_{z_2} + A(v) \tag{41}$$
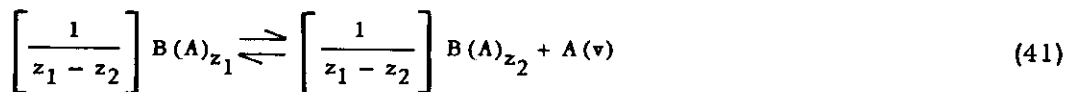
where $s \geq z_1 > z_2 \geq 0$

A schematic representation of the partial molar free energy of A versus composition for this system is shown in figure 27.

Several cases of the influence of diffusion on evaporation will be discussed. Schematic representation of the net rate of loss of material due to evaporation, the time dependence of the concentration of A through the sample, and the time dependence of the evaporation for these cases are shown in figures 28 through 33.

At time $t = 0$, the start of the evaporation, the concentration is uniform throughout the sample. The case is being considered where the initial concentration is
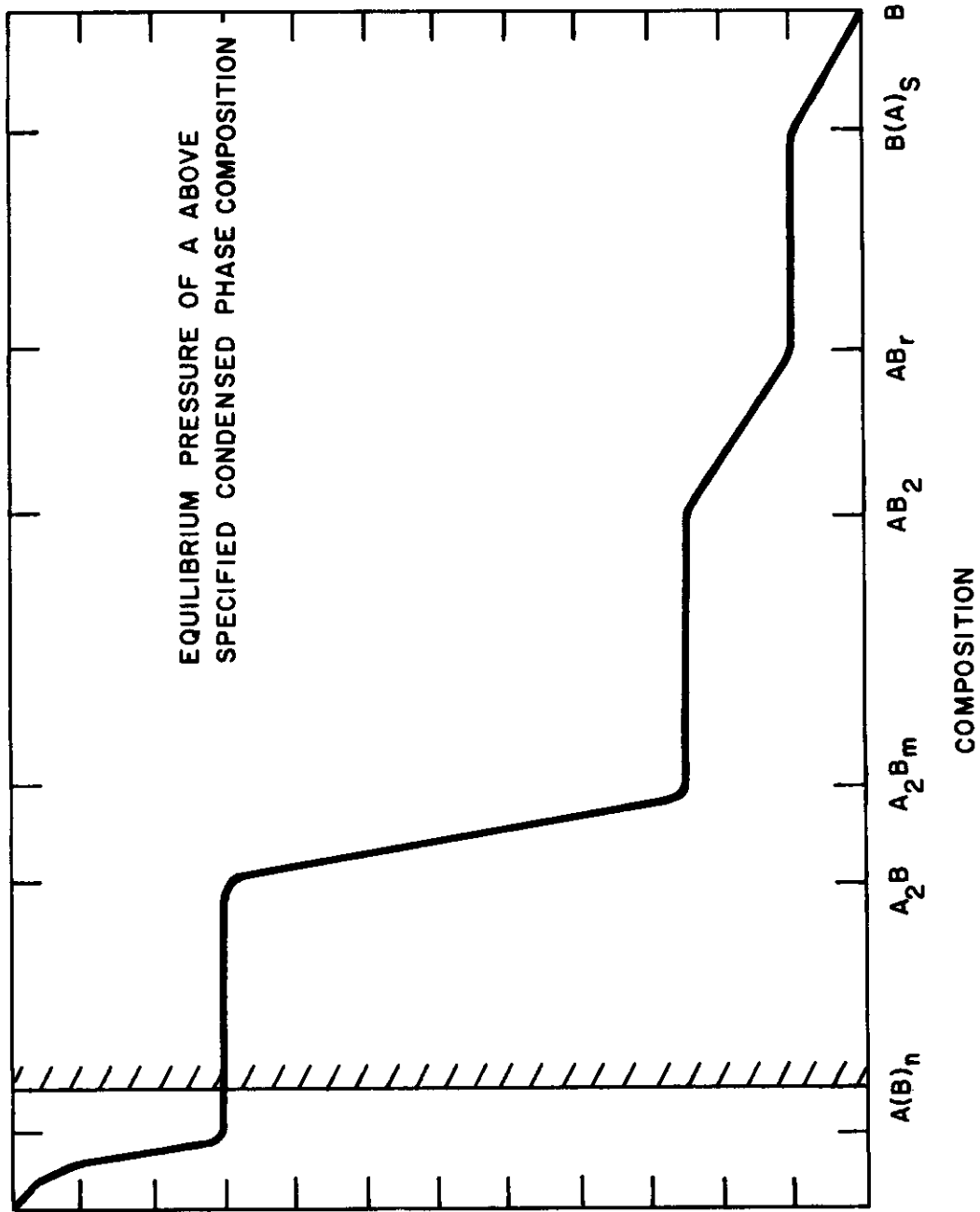
WADD TR 60-463 Pt. II   -72-

EQUILIBRIUM PRESSURE OF A ABOVE
SPECIFIED CONDENSED PHASE COMPOSITION

COMPOSITION

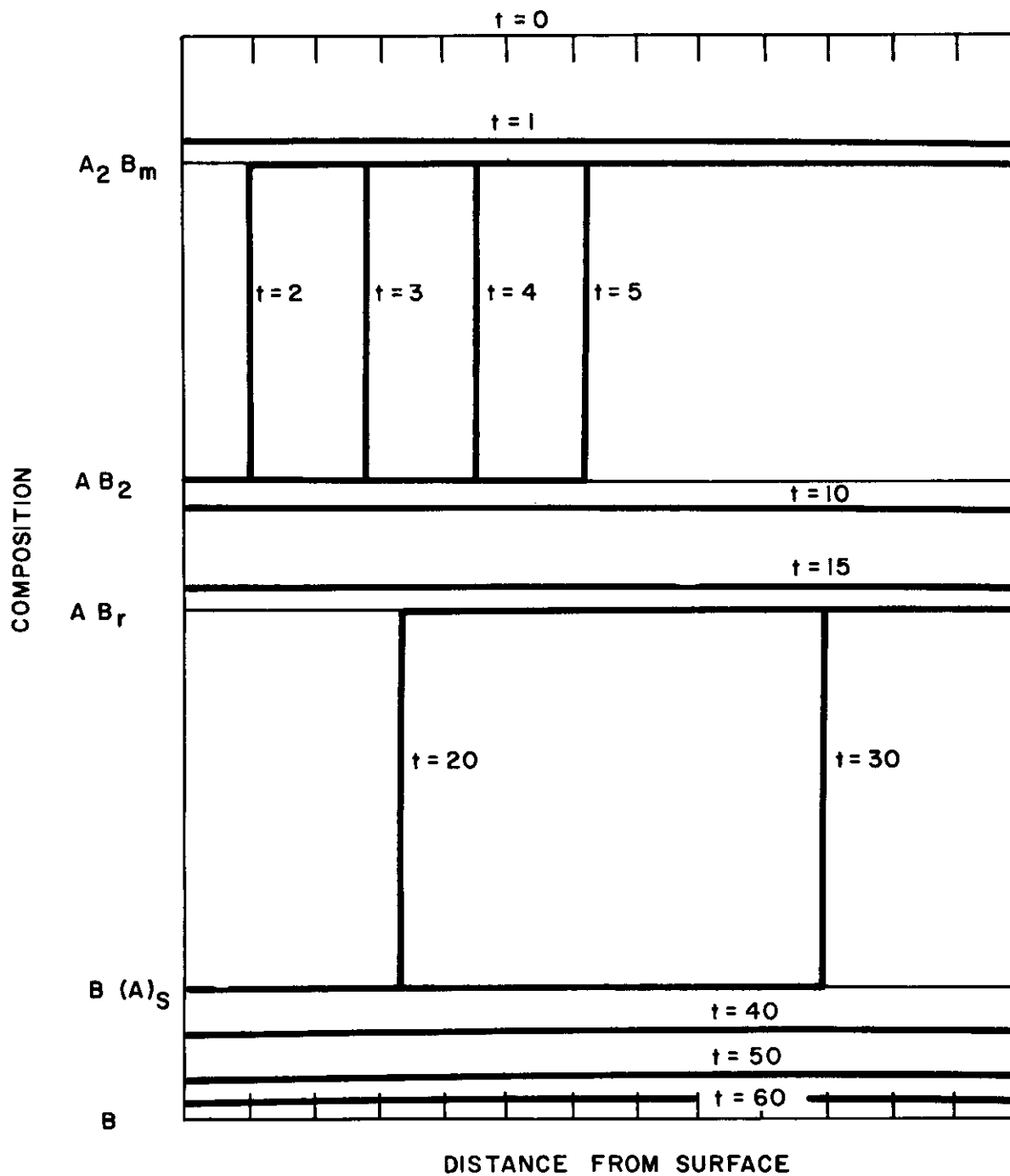Figure 27 Equilibrium pressure versus composition

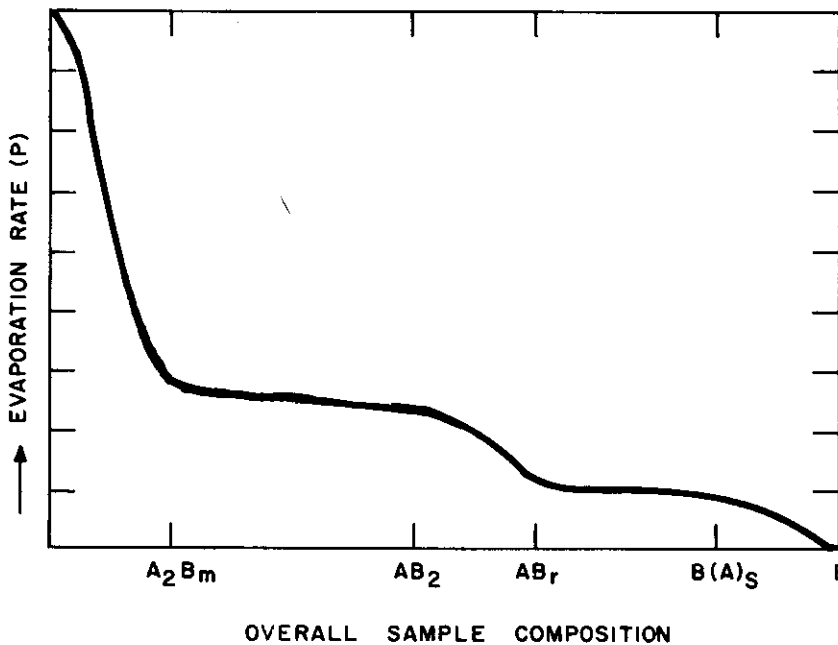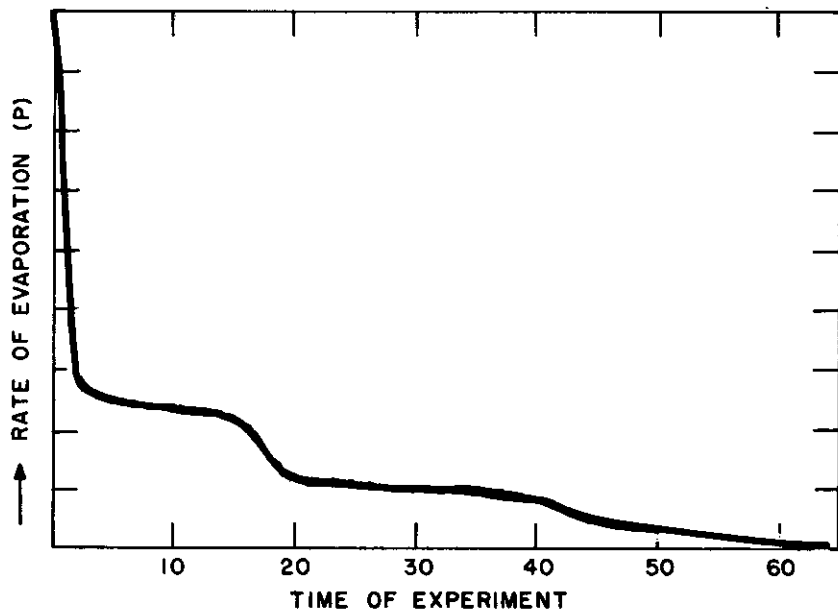Figure 28 Case I composition as a function of distance
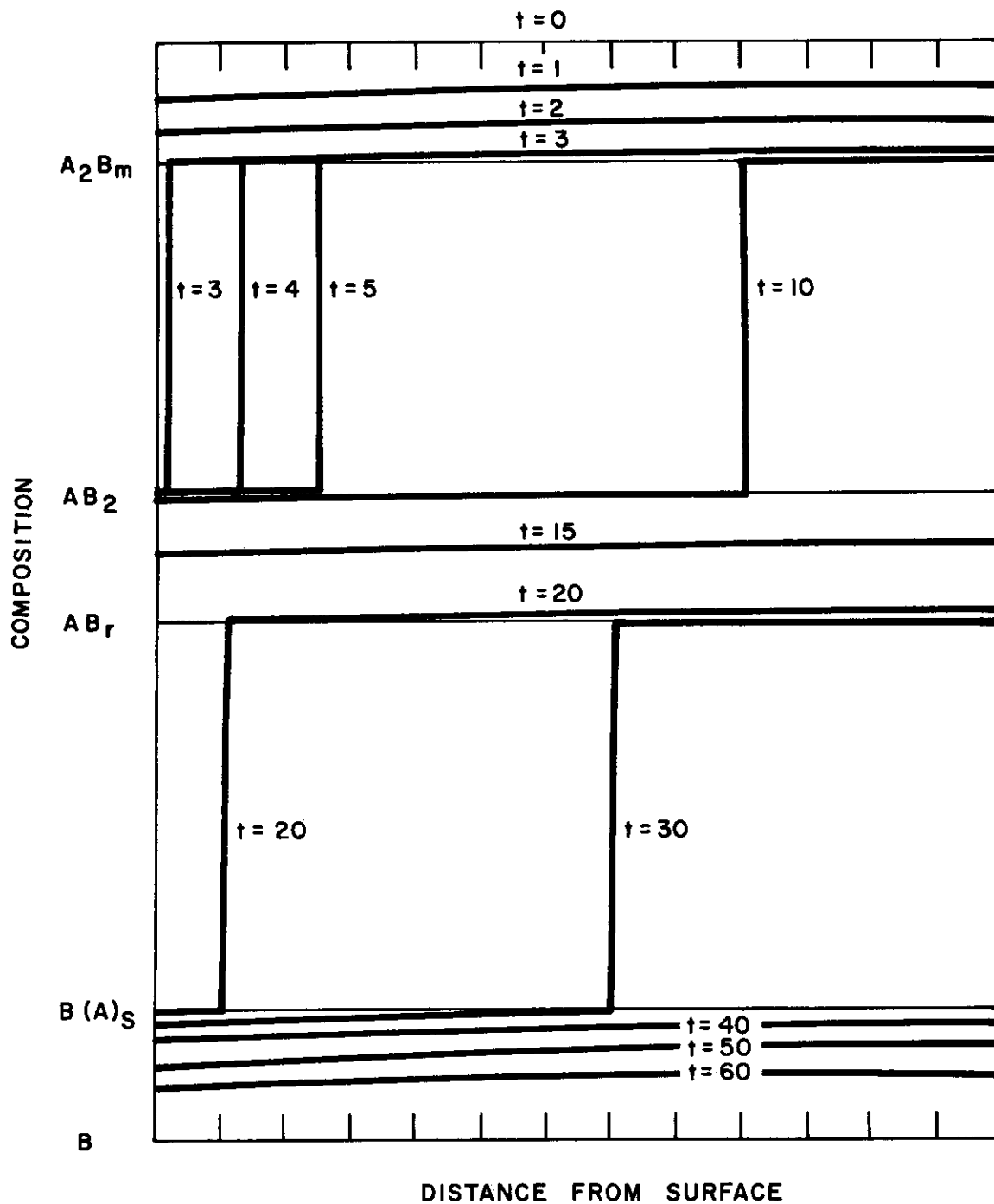
Figure 29 Case I rate of evaporation

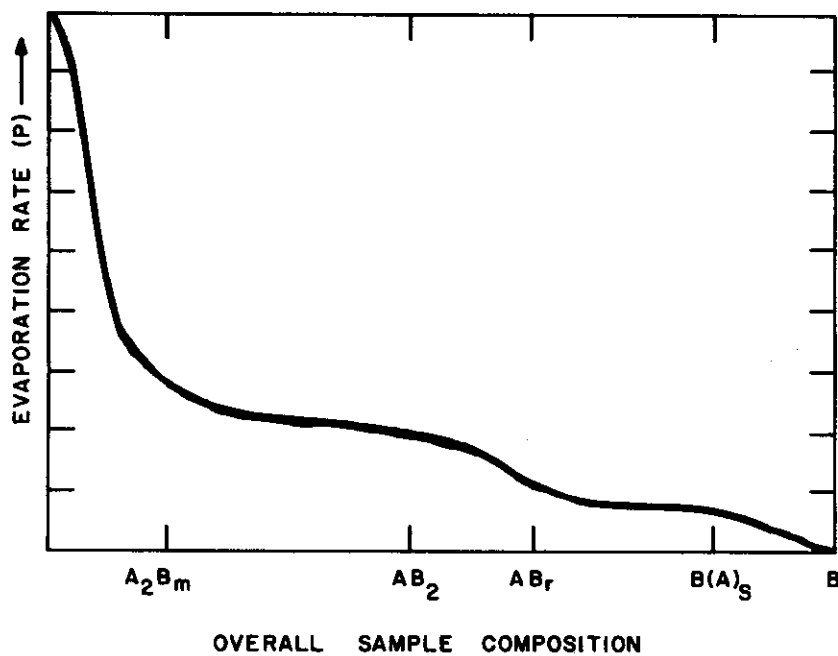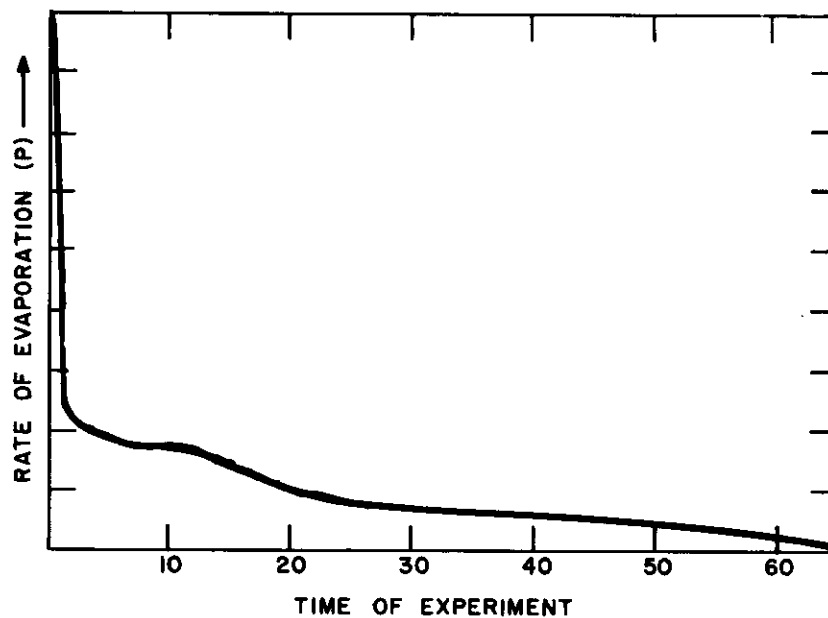Figure 30 Case II composition as a function of distance

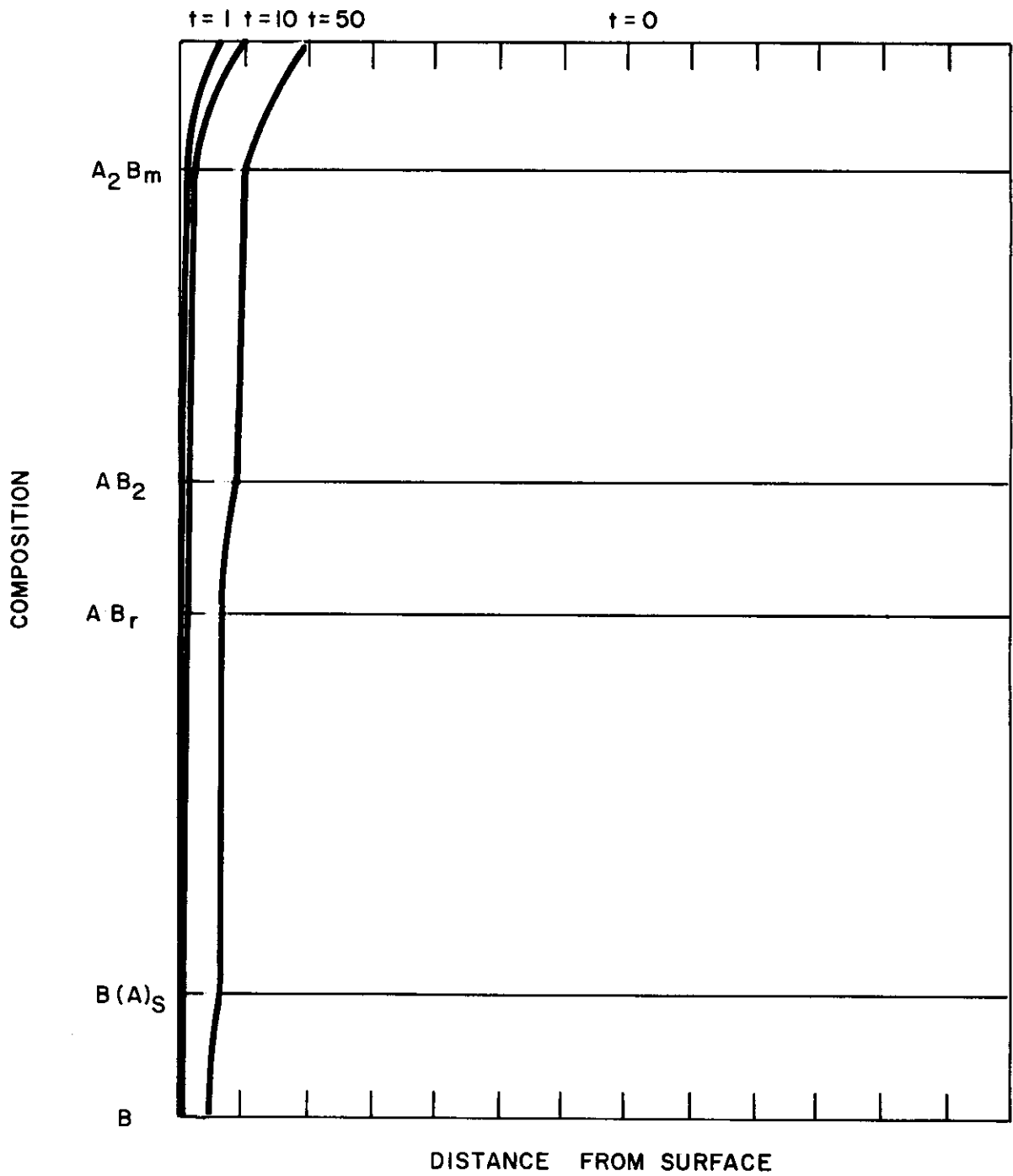Figure 31 Case II rate of evaporation

Figure 32 Case III composition as a function of distance
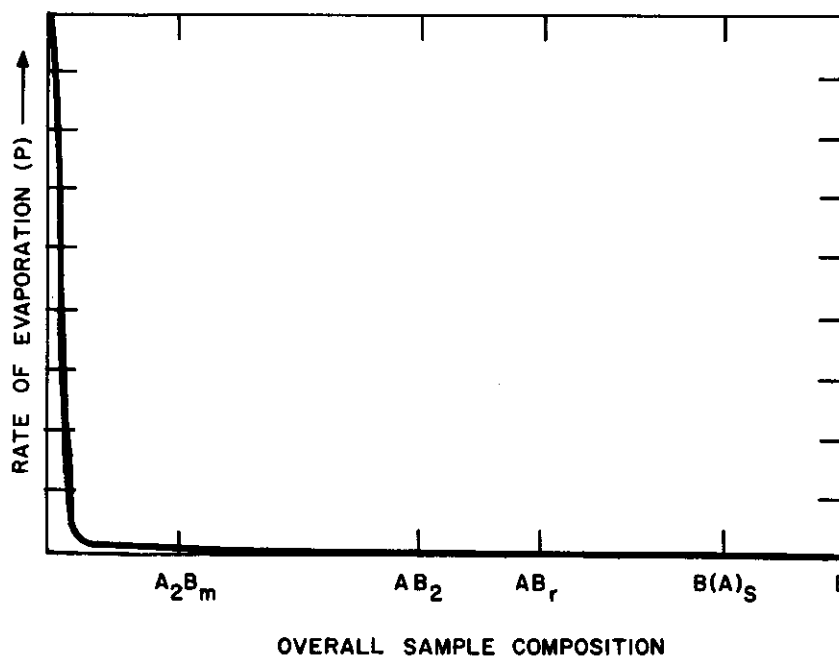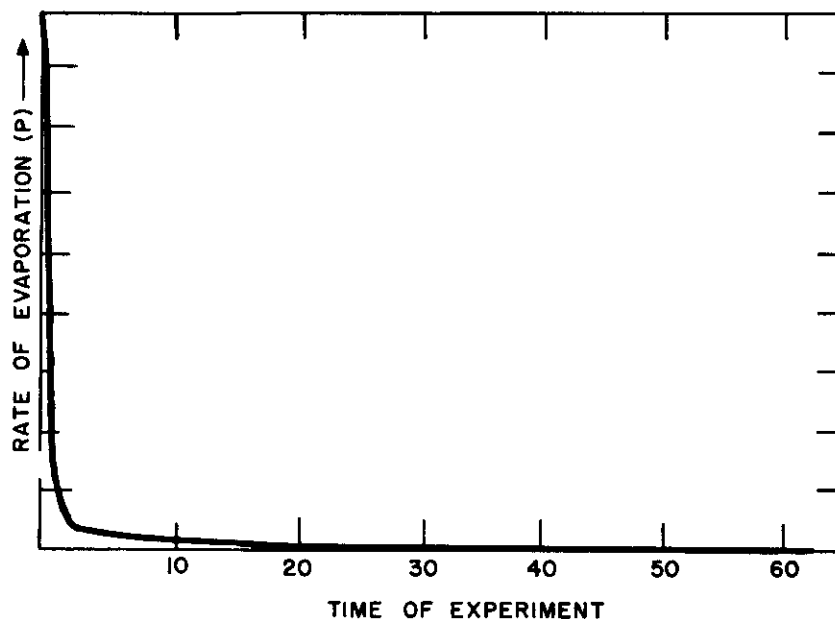
Figure 33 Case III rate of evaporation

in the A_2B phase field. As atoms leave the surface, a concentration gradient is set up. This causes atoms from the interior to diffuse toward the surface to relieve this concentration gradient. This continues until the surface composition reaches A_2B_m. At this point, its free energy is equal to that of AB_2, and it may undergo the reversible phase change reaction to form AB_2 as A evaporates. For the cases under discussion, the phase change reactions will not be considered as rate limiting.

Any local region of the $A-B$ system can exist in only one of four crystal structures, A, A_2B, AB_2, or B if metastable states are not considered. Thus, when the region containing A_2B_m undergoes a phase change due to the loss of A by evaporation, it goes directly to a phase with the AB_2 structure and composition, with no intermediate state being possible. The region over which a phase change takes place is assumed to be narrow for the systems of interest to the present discussion.

Similar reasoning can be applied to the AB_2 phase region. The surface concentration can vary continuously until it reaches AB_r, at which point any further evaporation of A produces the new structure $B(A)_s$. Continued evaporation of A will ultimately yield pure B.

The exact rates of evaporation and composition dependence of the sample with time depends upon the relative rates of evaporation, diffusion and phase change reaction. Each of these quantities is concentration dependent. The mathematics for the analogous case of diffusion of gases into a condensed phase with chemical reaction has been worked out (refs. 37, 38, 39). These detailed calculations will not be used but, rather, intuitive arguments for the case where phase nucleation and reaction are fast will be discussed.

Figures 28 and 29 describe the case where diffusion is almost able to keep up with evaporation. Figures 30 and 31 describe the case where diffusion is slower, and Figures 32 and 33 where it is still slower. It should be noticed that these are all specific points in the same general relationship.

The previous arguments have indicated that with a knowledge of the concentration gradients of the volatile constituents through the sample, continuous monitoring of the rate of evaporation may be used to obtain equilibrium partial molar free energies. Also, by means of X-ray diffraction, metallographic analysis, and chemical analysis, it may prove, in many cases, easier to obtain this information than to maintain conditions that have been considered necessary in the past to conduct effusion experiments. This especially may be true where a container material is not available, and only Langmuir experiments can be performed.

The types of systems that can be investigated by the continuous weighing method, using the above considerations are:

1.   The study of binary systems where one component is a liquid, and one component is the crucible, e.g,, one can measure the rate of evaporation of silicon from silicon contained in a tungsten crucible (to obtain the dissociation pressures of W – Si system).

2.   The study of binary systems in which one component has been applied directly to the crucible as a coating (the crucible being the other component of the system), e.g., one can measure the rate of evaporation of boron from a tantalum crucible whose inside is coated with boride (to obtain the dissociation pressures of the Ta – B system).

REFERENCES

1. Hasapis, A.A., M.B. Panish, and C. Rosen, The Vaporization and Physical Properties of Certain Refractories, Part 1, WADD-TR-60-463 (October 1960).

2. Stull, D.R. and G.C. Sinke, Thermodynamic Properties of the Elements, American Chemical Society, Washington, D.C. (1956).

3. Brewer, L. and M.S. Chandrasekharaiah, Free Energy for Gaseous Monoxides, UCRL-8713 (April 1959).

4. Brewer, L., Chapter 7 of an unpublished compilation (Revised September 1960).

5. Searcy, A.W., J. Am. Ceram. Soc. 40, 431 (1957).

6. Hansen, M., Constitution of Binary Alloys, McGraw-Hill (1958).

7. Aronsson, B., Acta Chem. Scand. 9, 1107 (1955).

8. Searcy, A.W. and A.G. Tharp, J. Phys. Chem. 64, 1539 (1960).

9. Schwartzkopf, P. and R. Kieffer, Refractory Hard Metals, Macmillan (1953).

10. Argonne National Laboratory, Chem. Eng. Quarterly Reports (1956, 1957).

11. Dorsey, N.E., J. Wash. Acad. Sci. 18, 505 (1928).

12. Norton, F.H., W.D. Kingery, G. Economos and M. Humenick, Jr., Massachusetts Institute of Technology Report NYO-3144 (1953).

13. Bashforth and Adams, An Attempt to Test the Theories of Capillary Action, Cambridge (1893).

14. Taylor, H.J. and J. Alexander, Proc. Indian Acad. Sci. 19A, 149 (1944).

15. Coghill and J. Anderson, J. Phys. Chem. 22, 245 (1918).

16. Kingery, W.D., Massachusetts Institute of Technology, Private Communication.

17. Langmuir, I., Phys. Rev. 2, 239 (1913).

18. Knudsen, M., Ann. Physik 29, 179 (1909).

19. Campbell, I. E., High Temperature Technology, John Wiley and Sons, New York (1956).

20. Inghram, M. G. and J. Drowart, Proceedings of the International Symposium on High Temperature Technology, 6 to 9 October 1959, McGraw-Hill, New York (1960), p. 219.

21. Panish, M. B. and L. Reif, The vaporization of iridium and rhodium, J. Chem. Phys. 34, 1915 (1961).

22. Dushman, S., Scientific Foundations of Vacuum Technique, John Wiley and Sons, New York (1949).

23. Margrave, J. L., J. Chem. Educ. 32, 520 (1955).

24. Hampson, R. S. and R. F. Walker, National Bureau of Standards (private communication).

25. Drowart J., G. DeMaria, R. P. Burns, and M. G. Inghram, J. Chem. Phys. 32, 1366 (1960).

26. Otvos, J. and D. Stevenson, J. Am. Chem. Soc. 78, 546 (1956).

27. Chupka, W. A., M. G. Inghram, and R. F. Porter, J. Chem. Phys. 24, 792 (1956).

28. Walsh, P. N., H. W. Goldstein, and D. White, J. Am. Ceram. Soc, 43, 229 (1960).

29. Panish, M. B. and L. Reif, op cit, p. 1079.

30. Yost, D. M., H. Russel, Jr., and C. S. Garner, The Rare Earth Elements and Their Compounds, John Wiley and Sons, New York (1947).

31. Ditchburn, R. W. and J. C. Gilmour, Revs. Modern Phys. 13, 310 (1941).

32. Darken, L. S. and R. W. Gurry, Physical Chemistry of Metals, McGraw-Hill (1953).

33. Speiser, R. and H. L. Johnston, Trans. Am. Soc. Met. 42, 306 (1950).

34. Valekis, E., C. L. Rosen, and H. M. Feder, J. Phys. Chem. 65, 2127 (1961).

35. Ackerman, R. J., Argonne National Laboratory Report 5482.

36. Blackburn, P. E., J., Phys. Chem. 62, 897 (1958).

37. Wilson, A. H., Phil. Mag. 39, 48 (1948).

38. Crank, J., Phil. Mag. 39, 362 (1948).

39. Jost, W., Diffusion in Solids Liquids and Gases, New York Academic Press (1952).